

# Abundances of Baade's Window Giants from Keck/HIRES Spectra: I. Stellar Parameters and [Fe/H] Values<sup>1</sup>

Jon. P. Fulbright

*Observatories of the Carnegie Institution of Washington, 813 Santa Barbara St., Pasadena, CA 91101*

`jfulb@ociw.edu`

Andrew McWilliam

*Observatories of the Carnegie Institution of Washington, 813 Santa Barbara St., Pasadena, CA 91101*

`andy@ociw.edu`

R. Michael Rich

*Division of Astronomy, Department of Physics and Astronomy, UCLA, Los Angeles, CA 90095-1562*

`rmr@astro.ucla.edu`

## ABSTRACT

We present the first results of a new abundance survey of the Milky Way bulge based on Keck/HIRES spectra of 27 K-giants in the Baade's Window ( $l = 1$ ,  $b = -4$ ) field. The spectral data used in this study are of much higher resolution and signal-to-noise than previous optical studies of Galactic bulge stars. The [Fe/H] values of our stars, which range between  $-1.29$  and  $+0.51$ , were used to recalibrate large low resolution surveys of bulge stars. Our best value for the mean [Fe/H] of the bulge is  $-0.10 \pm 0.04$ . This mean value is similar to the mean metallicity of the local disk and indicates that there cannot be a strong metallicity gradient inside the solar circle. The metallicity distribution of stars confirms that the bulge does not suffer from the so-called "G-dwarf" problem. This paper also details the new abundance techniques necessary to analyze very metal-rich K-giants, including a new Fe line list and regions of low blanketing for continuum identification.

*Subject headings:* stars: abundances;

## 1. Introduction

We have been engaged in a long term program using high-resolution spectroscopy to study the composition of stars in the Galactic bulge, with the aim of constraining the conditions of the bulge’s formation and chemical evolution at a level of detail that is impossible to obtain with any other method. Our plan is to obtain high S/N spectra for samples of >20 stars in each of 3 latitudes in the bulge: Baade’s Window ( $b=-4^\circ$ ), Sgr I ( $b=-2.65^\circ$ ), and the Plaut field ( $b=-8^\circ$ ). This paper describes the beginning of the analysis of the Baade’s Window sample based on Keck/HIRES data; the observations and analysis of the other two fields, taken with Magellan/MIKE, will be described in future papers.

The full sample will enable the homogeneity of the chemical properties of the bulge to be investigated, which may reveal evidence of galactic accretion, or multiple star formation events. Pertinent questions might include: What are the metallicity and composition gradients in the Galactic bulge, and how do they constrain bulge formation scenarios. Did some fraction of the population form in separate systems that merged very early on? What fraction of the population might have originated in a system similar to the Sagittarius dwarf spheroidal galaxy? Are there correlations between kinematics and composition, and do the composition gradients differ from the iron abundance gradient?

The fossil record of the Local Group is important because we cannot trace, with certainty, the evolution of distant galaxies or populations in distant galaxies to the present epoch. In order to understand the formation of galaxies, such as our own, we must also use the constraints available from the ages, kinematics, and chemistry of stars in its constituent stellar populations. This is especially true if present day galaxies accumulated through a complicated set of mergers, as suggested in the CDM galaxy formation scenarios (e.g., Kauffmann 1996). K-giants provide useful probes for understanding chemical evolution because they are luminous, cover the full range of possible ages, contain lines from many elements, and, except for a few light elements, they preserve the composition of the gas from which they were formed. The widely accepted paradigm (Tinsley 1979; Wheeler et al. 1989; Timmes et al. 1995; McWilliam 1997) is that yields of massive star Type II SNe are enriched in alpha elements (e.g. O, Mg, Si, Ca, Ti), and the longer-timescale Type Ia SNe are enriched in iron. Consequently, the relative importance of alpha elements and iron gives a constraint on the enrichment timescale for the stellar population. For example, Elmegreen (1999) models bulge formation as a maximum intensity star burst that concludes in  $10^8$  yr.

---

<sup>1</sup>Based on data obtained at the W. M. Keck Observatory, which is operated as a scientific partnership among the California Institute of Technology, the University of California, and NASA, and was made possible by the generous financial support of the W. M. Keck Foundation.

The consequences for chemical evolution were modeled by Matteucci et al. (1999), who predicted abundance trends in the bulge for a wide range of elements. The expectation is that the rapid formation of the bulge should produce an over-enhancement of alpha elements. However, all elements are of interest because different families of elements are thought to be made under a variety of astrophysical circumstances, which can provide information on the bulge environment during its formation, and may also lead to a greater understanding of nucleogenesis. Surveys of large samples of stars in globular clusters and dwarf spheroidal galaxies are just beginning, and our research will add the study of the bulge population to these efforts.

The earliest efforts to obtain spectra of bulge K-giants with digital detectors were by Whitford & Rich (1983) and Rich (1988; hereafter R88). These studies concluded that there is a range of metallicity in the bulge and found evidence for super-metal-rich stars. R88 found the mean abundance for the bulge was  $[\text{Fe}/\text{H}] \sim +0.2$ . McWilliam & Rich (1994; hereafter MR94) obtained marginal high-resolution echelle spectroscopy ( $R=17,000$ ,  $S/N \sim 50$ ) of 11 bulge K-giants from the sample of R88 using the CTIO Blanco 4-m telescope and revised the abundance distribution in the bulge downward. The results of MR94 were used to re-calibrate the Rich (1988) low-resolution sample, and indicated a mean abundance of  $[\text{Fe}/\text{H}] = -0.25$ . MR94 also found enhancements of the alpha elements Mg and Ti, even for stars with the solar iron abundance. The alpha elements Si and Ca did not appear to be enhanced over the solar neighborhood trends; this was explained by MR94, in the context of the supernova nucleosynthesis predictions of Woosley & Weaver (1995), as due to a top-heavy bulge IMF. These early studies were made difficult by the lack of accurate basic optical and infrared photometry for the bulge, and the large, but uncertain, reddening (now known to be highly variable). The high metallicity and cool temperatures of the bulge giants also posed difficulties due to blending, and because it was necessary to use lines with somewhat uncertain  $gf$ -values. In addition, the extreme stellar crowding in these low-latitude fields, and the faintness of the bulge stars, made it impossible to obtain the highest quality data with 4m-class telescopes; as a result, the use of relatively low resolving power spectra led to considerable blending with CN lines.

The first spectrum of a bulge giant with Keck (Castro et al. 1996) confirmed the metal-rich end of the MR94 abundance distribution; however, the spectrum was of low  $S/N$  and it was clear that a serious Keck telescope campaign was urgently needed. This effort has been underway since August 1998. Acquisition of the spectra has proceeded slowly, since we require  $S/N > 50$  and  $R > 45,000$ ; in fact, most of our spectra have  $R = 60,000$ .

An analysis of a subset of the new Keck spectra was given in Rich & McWilliam (2000; hereafter RM00). The analysis employed model atmosphere parameters based entirely on

the spectra rather than on photometry: effective temperatures were set by demanding that Fe I line abundances were independent of excitation potential, whilst the stellar gravities were chosen so that Fe I and Fe II abundances were equal. The RM00 abundances at the metal rich end are  $\sim 0.15$  dex more metal rich than MR94. The key results of MR94 were confirmed for the alpha elements:  $[\text{Mg}/\text{Fe}]$  and  $[\text{Ti}/\text{Fe}]$  are elevated, while Ca followed the disk abundance trend. Oxygen was clearly measured for the first time, and it was found that  $[\text{O}/\text{Fe}]$  declines rapidly above  $[\text{Fe}/\text{H}] = -0.5$ , a result that we will confirm with new work presented in a future paper.

One problem with the RM00 study was due to the sensitivity of the spectroscopic model atmosphere parameters to the adopted  $gf$ -values of the iron lines. In addition, the covariance between the spectroscopic temperature and spectroscopic gravity meant that a slight error in temperature returned a large error in gravity, which then required an additional adjustment in temperature, in the same direction as the original error. In this way it was possible to obtain spectroscopic parameters unexpectedly far from the true values.

McWilliam & Rich (2004; hereafter MR04) analyzed some of the same data as RM00 (and found here), but avoided the pitfalls found by RM00 by introducing two spectroscopic methods for deriving  $T_{\text{eff}}$  values. The first method derived temperatures based on the excitation of Fe I lines, with  $gf$ -values obtained from the analysis of the well-studied K-giant Arcturus; note that the Arcturus  $gf$ -values include systematic effects, such as the deficiencies of the adopted model atmosphere grid, and so are not necessarily equal to laboratory values. The second spectroscopic technique used for setting  $T_{\text{eff}}$  in MR04 is to force the ionization equilibrium between Fe I and Fe II lines using a gravity derived from photometric data and an assumed mass of  $0.8 M_{\odot}$ . These two new spectroscopic techniques were relatively robust, as well as insensitive to reddening uncertainties that might affect photometrically determined temperatures. The spectroscopic temperatures from MR04 compared extremely well with  $T_{\text{eff}}$  photometric temperatures derived using the Alonso (V–K) calibration and (V–K) colors based on 2MASS K and OGLE V data. In this work, we expand upon the improvements implemented in MR04.

The bulge stars studied here are located in Baade’s Window, a region of relatively low reddening ( $A_V \sim 1.3$  mag) located about 4 degrees from the direction of the Galactic center. If a galactocentric distance of 8 kpc is assumed (e.g. Merrifield 1992, Carney et al. 1995), then the closest approach of the line of sight to the Galactic center is about 550 pc. For comparison the scale height of the bulge is approximately 350 pc (Wyse et al. 1997). The star identifications we use for the bulge stars are those of Arp (1965).

In the present study we have employed two spectroscopic methods for estimating stellar parameters, and we check these with V–K colors derived from the newly available 2MASS

K-band magnitudes (Cutri et al. 2003) together with V-band measurements from the OGLE microlensing survey (Szymanski et al. 1996). These three methods provide excellent agreement in the stellar parameters, so we are confident that the present study currently provides the best approach for the detailed abundance analysis of bulge giants. We shall see that our results for the iron abundance scale now returns more closely to that of MR94 and MR04 than RM00.

In Section 2, we describe the observations and data reduction. In Section 3 we describe the basic problems in the analysis of metal-rich K-giants and outline our solutions. Section 4 contains a description of the new Fe line list needed for the analysis. Our continuum measurement and equivalent width measurement method are explained in Section 5, while the methods we use to obtain the stellar parameters are described in Section 6. The results of the analysis are provided in Section 7, including a discussion of stars for which the initial analysis failed. Finally, in Section 8 we use our results to recalibrate low resolution observations of Baade’s Window giants to rederive the metallicity distribution function.

## 2. Observations and Data Reduction

The observations of Baade’s Window stars reported here were taken with the HIRES spectrograph (Vogt et al. 1994) on the Keck I telescope between 1998 and 2001. The spectra were taken with the C1 (0.861 arcsec by 7.0 arcsec) and B2 (0.571 arcsec by 7.0 arcsec) slits yielding instrumental resolutions of 45000 and 60000, respectively. The higher resolution was used for the highest metallicity targets. The HIRES spectra roughly cover the wavelength range 5375 to 7875 Å, with inter-order gaps increasing to the red. The data were reduced with the MAKEE package from T. Barlow<sup>2</sup>. The reduced spectra have signal-to-noise (S/N) values between 45 and 100 per pixel. The journal of Keck observations is given in Table 1, and sample sections of three stars are displayed in Figure 1.

Echelle spectra of nearby giant stars were obtained with the du Pont 2.5-m telescope at Las Campanas and the 0.6-m CAT telescope at Lick Observatory. These stars were selected from McWilliam (1990) to have similar  $M_V$ ,  $[Fe/H]$  and  $T_{\text{eff}}$  values as the Baade’s Window sample. These data were taken to help check the methods used for determining the stellar parameters of the bulge giants. The du Pont echelle spectrograph has a resolution of about 30000, while the CAT at Lick Observatory uses the Hamilton spectrograph (Vogt et al. 1987)

---

<sup>2</sup>MAKEE was developed by T. A. Barlow specifically for reduction of Keck HIRES data. It is freely available on the world wide web at <http://spider.ipac.caltech.edu/staff/tab/makee/index.html> or <http://www2.keck.hawaii.edu/inst/hires/makeewww/>

delivers a resolution of about 45000. Both spectrographs give complete wavelength coverage in the 5000-8000 Å wavelength range. The HIRES spectrum of  $\mu$  Leo (HR 3905) was reduced using MAKEE, but the remainder of the stars were reduced using IRAF<sup>3</sup> routines. The data from the Las Campanas 2.5-m echelle were extracted, and scattered-light subtracted, using IRAF scripts written by AM. The S/N ratio of the disk spectra are very high, often over 200 per pixel. Details of these spectra are included in Table 2.

The sample of disk giants includes a Lick/CAT observation of Arcturus. In Sections 3 and 4 (and Tables 3 and 4) we use the Hinkle et al. (2000) Arcturus atlas to help develop the analysis method. In later sections, though, we analyze the Lick/CAT spectrum of Arcturus (HR 5340 in the Tables 7 and 9) just like the other disk stars. In this way, the Lick/CAT spectrum of Arcturus provides a consistency check showing how the lower resolution and S/N of the disk sample affects the results as compared to the atlas.

The bulge sample was selected to cover a wide metallicity range in order to investigate the chemical evolution of the bulge. Baade’s Window contains stars from populations other than the bulge (namely foreground disk and background halo stars). Fortunately, R88, MR94, and Sadler et al. (1996; hereafter SRT96) studied the relative fraction of non-bulge contaminants within Baade’s Window. Figure 10 of SRT96 shows the probability a star being a member of the bulge, disk or halo as a function of the observed V magnitude ( $V_{\text{obs}}$ ). This probability is a “worst-case” value for individual stars because it excludes any other information (color, metallicity, photometric parallax, etc.) that might be used to help further classify an individual star.

The bulge dominates the membership of stars with  $V_{\text{obs}}$  between about 15.5 and 18.0, with the disk being the main contaminant at brighter magnitudes. Between  $V_{\text{obs}}$  of 16.5 and 17.5, the probability of bulge membership rises to over 80 percent due to the presence of the bulge red giant branch clump in that magnitude range. Background halo stars are only a minor contaminant, with the maximum probability of contamination rising to just over 10 percent around  $V_{\text{obs}}$  of 16.1 mag. Halo stars are the main contaminant in the regime of bulge RGB clump stars, but it is likely the halo stars are confined to the lowest metallicities.

For the stars observed here, the  $V_{\text{obs}}$  values place only 10 stars in regions where probability of bulge membership is less than 80 percent. Of those, all 10 are either individually identified by SRT96 as bulge members due to photometric parallax or were observed by MR94 and previously confirmed having distances consistent with bulge membership. There-

---

<sup>3</sup>IRAF is distributed by the National Optical Astronomy Observatories, which are operated by the Association of Universities for Research in Astronomy, Inc., under cooperative agreement with the National Science Foundation.

fore, in our initial analysis we can assume that all the stars we observed in Baade’s Window are bulge members (we test this assumption in Section 7.1).

It has been noted by SRT96 that velocity information is not very useful as a population diagnostic in Baade’s Window. They find that the velocity dispersions for the bulge, disk and halo in Baade’s Window to be 103, 82 and 149 km/s, respectively. Rich (1990) found a bulge velocity dispersion of  $104 \pm 20$  km/s.

### 3. Difficulties in the Analysis of Metal-Rich Giants

The bulge is distant ( $\approx 8$  kpc) and heavily reddened ( $A_V \sim 1.3$  mag in Baade’s Window). The only stars that can be analyzed in large numbers at high-resolution and S/N are intrinsically bright giants. But the bulge is also metal-rich, with a mean metallicity of roughly solar (see SRT96 and Section 7). Bright, metal-rich giants suffer from heavy line blanketing, and many of the well-studied lines with high quality laboratory  $gf$ -values are very strong. For example, the line list of Fulbright (2000) is based on Fe I lines from the Oxford group (Blackwell et al. 1989 and references therein) and O’Brian et al (1991). When these lines are measured in the nearby metal-rich K-giant  $\mu$  Leo, there are only 36 unblended Fe I lines weaker than  $150 \text{ m}\text{\AA}$  available in the wavelength region observed, and only 11 of those are weaker than  $90 \text{ m}\text{\AA}$ .

But there are also more basic difficulties affecting even the analysis of metal-poor giants. For Arcturus, Smecker-Hane & McWilliam (2002; 2004 unpublished) found a disconcerting 110 K difference between the physical  $T_{\text{eff}}$  (based on the known flux, distance and angular diameter) and  $T_{\text{eff}}$  based on Fe I excitation ( $T_{\text{Ex}}$ ). This difference was reduced to 40 K if a group of high-excitation Fe I lines was excluded from the analysis, and suggests problems with the Fe I  $gf$ -values, or blends, at red wavelengths. The remaining 40 K difference may be due to problems with the upper layers of the model atmospheres, where the empirical  $T$ - $\tau$  relation for Arcturus (Ayres & Linsky 1975) differs significantly from the Kurucz (1993) model (see also McWilliam et al. 1995a).

As an example of the problems encountered, we can conduct a simple analysis for the slightly metal-poor bulge star I-194. First, we used the line list of MR94 (with the addition of a few Fe II lines from Fulbright 2000) and measured 82 equivalent widths using the IRAF *splot* package and fitting the continuum by eye. For the purposes of this example only, we set the  $T_{\text{eff}}$  value using the excitation method and set  $\log g$  by forcing ionization equilibrium between Fe I and Fe II.

When this is done, we find  $T_{\text{eff}} = 4490$  K,  $\log g = 1.45$ ,  $[m/H] = -0.10$ , and  $v_t =$

1.45 km/s, which requires  $M_{\text{Bol},*} = +0.95$ , or a distance of 5.9 kpc—well outside the bulge. If we force a distance of 8 kpc, then the ionization difference ( $\log \epsilon(\text{Fe II}) - \log \epsilon(\text{Fe I})$ ) jumps to  $-0.42$  dex. The photometric  $T_{\text{eff}}$  ( $T_{\text{Phot}}$ ; see Sections 6.2-6.4 for details on how we determine stellar parameters) for this star is 4153 K, or 337 K cooler, and if we assume a distance of 8 kpc, the ionization difference is  $+0.21$  dex. Ionization equilibrium at this  $T_{\text{eff}}$  requires a distance of 15.0 kpc, far on the other side of the bulge. The range of  $[\text{Fe}/\text{H}]$  values from all the above parameter determinations range from  $-0.42$  to  $-0.04$ .

Except for the wish to have the star located in the bulge, there are no additional constraints on the parameters. Both  $T_{\text{Phot}}$  and  $T_{\text{Ex}}$  methods are valid in theory, but the actual application here has led to discordant results. In Figure 2 we plot excitation plots from both  $T_{\text{eff}}$  methods based on the 8 kpc results. In the lower panel, it appears that the removal of certain lines might flatten the slope of the Fe I lines and bring Fe II into agreement with Fe I. Indeed, the final  $T_{\text{eff}}$  we adopt for I-194 is 4176 K, but there is no evidence here to support the removal of those individual lines. In other stars the lines that are outliers in this plot are near the mean, and other lines are outliers. These lines also do not show any suspicious properties in the observed spectrum of I-194 that might explain their outlier status.

There are several reasons for the wide range of results for this star. As mentioned in the Introduction, excitation temperatures and ionization-based surface gravities exhibit a covariance. When  $T_{\text{eff}}$  is raised, the difference  $\log \epsilon(\text{Fe II}) - \log \epsilon(\text{Fe I})$  decreases. This forces an increase in the surface gravity, which in turn changes the slope of the excitation plot slightly, requiring another rise in  $T_{\text{eff}}$ .

Further, the list has a large number of strong lines in this star. There are only 15 lines weaker than 50 mÅ and 20 stronger than 120 mÅ. Abundances determined from strong lines depend greatly on the value of the microturbulent velocity ( $v_t$ ). Of the 15 weaker lines, 13 have excitation potentials of greater than 4 eV. These high-excitation lines are sensitive to  $T_{\text{eff}}$  changes, so a change in  $T_{\text{eff}}$  forces  $v_t$  changes. One can choose not to use stronger lines, but this greatly decreases the size of the line list and makes the analysis vulnerable to a few pathological lines. As mentioned in the example of  $\mu$  Leo above, the number of weak lines with high-quality  $gf$ -values available rapidly decreases at high metallicity. Some of the bulge giants have metallicities over 3 times that of I-194.

Finally, the abundance results for individual lines display a sizable line-to-line scatter (about 0.20 dex for Fe I and about 0.27 dex for Fe II). This kind of uncertainty can be due to errors in  $gf$ -values, unresolved blends in the spectrum (although MR94 attempted to use unblended lines), and problems in continuum determination. Uncertainties this large can reduce the diagnostic power of the parameter-determining methods, especially if only a few

lines are involved.

Problems like those detailed above convinced us to develop new techniques to analyze the giants in our sample. The need for more Fe lines and reduced line-to-line scatter drove us to create a new line list. Worries about the effects of blanketing on the continuum level induced us to create a new method to set the continuum. And the inability to independently select one  $T_{\text{eff}}$  diagnostic as superior made us use three different methods to set the parameters.

This development took several iterations to get to the final state, which makes describing the methods in a linear fashion difficult. For example, we use stellar parameters (Section 6) to synthesize the continuum regions (Section 5) so we can measure the Fe lines (Section 4), but we need a good set of Fe lines before we can set the stellar parameters. In the end, we analyzed each star at least four different ways before performing a final analysis.

#### 4. Line List

As stated above, one difficulty in the analysis of very metal-rich giants is that many of the well-studied lines with high quality laboratory  $gf$ -values are very saturated, with only a mild sensitivity to abundance. Additionally, the weaker lines all have high excitation potentials, while the stronger lines are from lower excited states. This sets up the possibility for correlated errors between the microturbulence velocity ( $v_t$ ) and the  $T_{\text{eff}}$  value when the  $T_{\text{eff}}$  value is determined by the slope of the  $\log \epsilon(\text{Fe I})$  versus excitation potential distribution (which we will refer to hereafter as the “excitation plot”). This can be alleviated by having a range of line strengths at all excitation potentials.

As mentioned in the previous section, McWilliam et al. (1995) also notes that Fe lines with strengths over  $\log(\text{RW}) = \log_{10}(W_\lambda/\lambda) \sim -4.7$  ( $\sim 120 \text{ m}\text{\AA}$  near  $6000 \text{ \AA}$ ) in very metal-poor stars suffer from the effects of improper modeling of the outer layers in many stellar atmosphere models. We therefore wish to exclude strong lines because we cannot rely on the abundance results from these lines. In addition, strong lines are sensitive to the selection of the microturbulent velocity. We found that in the example of the Fulbright (2000) list and  $\mu$  Leo, the mean abundance of the Fe I lines could change by 0.1 dex for every 0.1 km/s change in  $v_t$ . Due to the lack of weak lines, setting the value of  $v_t$  using the  $\log \epsilon(\text{Fe I})$  vs.  $\log(\text{RW})$  could lead to  $v_t$  uncertainties of up to 0.3 km/s in the stronger-lined stars. This situation is unacceptable and a new line list with more weak lines is required.

Our goal was to create a list of Fe I and Fe II lines that span a range of line strengths and excitation potentials that are unblended and are of appropriate strength ( $\sim 10\text{--}120 \text{ m}\text{\AA}$ ) for the range of metallicities found in the bulge giants. To find these lines, we used the spectrum

synthesis program MOOG (Snedden 1973) and the complete Kurucz line list “gfall.dat”<sup>4</sup> combined with the CN line list from MR94 to calculate the estimated EW values in small ( $\pm 2 \text{ \AA}$ ) wavelength regions around over 5500 Fe I and Fe II lines between 5400–7900  $\text{\AA}$ .

We used stellar parameters to simulate Arcturus ( $T_{\text{eff}} = 4290 \text{ K}$ ,  $\log g = 1.60$ ,  $[\text{m}/\text{H}] = -0.50$ , and  $v_t = 1.67 \text{ km/s}$ ), and a hypothetical giant with parameters identical to Arcturus, but with  $[\text{m}/\text{H}] = +0.5$ .

For the Arcturus  $T_{\text{eff}}$  value we employed the limb-darkened angular diameter of  $20.91 \pm 0.08 \text{ mas}$  from Perrin et al. (1998), which is in good agreement with the values in the range from  $20.78 \pm 0.31$  to  $21.04 \pm 0.05 \text{ mas}$  found by Quirrenbach et al. (1998). To compute  $T_{\text{eff}}$  from the angular diameter the bolometric flux is required; we utilized four measurements of the bolometric flux of Arcturus, from Augason et al. (1980), Bell & Gustafsson (1989), Alonso et al. (1999), and Blackwell et al. (1990). The median bolometric flux from these works is  $4.95 \times 10^{-12} \text{ W/cm}^2$ . The Hipparcos catalog lists the distance to Arcturus at  $11.25 \pm 0.09 \text{ pc}$ ; at this close distance it is safe to assume that there is no significant interstellar reddening, although the existence of circumstellar reddening is difficult to rule out. The median bolometric flux, listed above, indicates  $T_{\text{eff}} = 4294 \text{ K}$  for Arcturus. The Alonso et al. (2000) bolometric flux value is significantly lower than all other estimates, and indicates  $T_{\text{eff}} = 4268 \text{ K}$ , while the highest bolometric flux is from Bell & Gustafsson (1989), consistent with  $T_{\text{eff}} = 4337 \text{ K}$ . Thus, we adopt a  $T_{\text{eff}}$  value of  $4290 \text{ K}$ , close to the value of  $4280 \text{ K}$  determined by McWilliam (1990); we estimate the  $1\sigma$  at  $\sim 10$  to  $15 \text{ K}$ .

The absolute luminosity of Arcturus was determined from the observed V-band magnitude, bolometric corrections, and the Hipparcos distance of  $11.25 \text{ pc}$ . The mass was estimated at  $0.90 M_{\odot}$  from the location of Arcturus in the temperature-luminosity diagram, by comparison with the Padova theoretical isochrones (Girardi et al. 2000). From Equation 1 and the isochrone mass we compute the surface gravity for Arcturus, at  $\log g = 1.55$ , rounded to 1.6.

Our choice of parameters for Arcturus agree with other analyses (Griffin & Lynas-Gray 1999; Peterson et al. 1993).

In our syntheses, Kurucz model atmospheres (interpolated from the grid points using a program given to us by J. Johnson) with solar abundance ratios were used, but the abundance of  $[\text{C}/\text{Fe}]$  and  $[\text{N}/\text{Fe}]$  were changed to be  $-0.2$  and  $+0.4 \text{ dex}$ , respectively; this is typical of

---

<sup>4</sup>The most recent versions of the Kurucz line list and atmosphere grids can be found at <http://kurucz.harvard.edu/>. For the selection of the line list the solar-ratio grid with overshooting was used. See section 6.1 for a comparison of how the choice of atmosphere model grid affects the final results.

solar neighborhood red giant stars, which have altered their surface composition via dredge-up of material that has undergone nuclear processing in the stellar interior (e.g. Lambert & Ries 1981). The change in the [C/Fe] and, especially, [N/Fe] ratios affects the strength of CN features in our spectra.

The vast majority of the Fe lines considered are too weak, too strong, or too blended with other lines to be useful in our abundance analysis. Selected lines must have a simulated EW of over 2 mÅ in Arcturus and less than 150 mÅ in the [Fe/H] = +0.5 giant. We consider a line too blended if the sum of the lines within 0.2 Å of the center of the Fe line contribute more than 0.05 dex to the resulting log(RW) value of the blend. Further, we inspect the actual spectrum of  $\mu$  Leo to ensure that no unaccounted lines in the synthesis contaminate the Fe line of interest. We note that our list of clean Fe I lines is restricted by the coverage of the  $\mu$  Leo spectrum; additional lines may be identified in later studies. The line list presented here is made up of the Fe lines with the least amount of stellar or telluric contamination possible in the wavelength regions observed. The final result is a list of 154 Fe I lines and 5 Fe II lines.

Most of these lines, however, do not have laboratory  $gf$ -values available. We have therefore chosen to conduct our analysis differentially from the well-studied giant Arcturus. A differential analysis also helps reduce systematic errors, such as deficiencies in the model atmospheres and the effects of weak blends that scale with metallicity.

The differential abundance analysis was performed on a line-by-line basis for a subset of our Fe lines, which we believe to be least affected by blends, with strengths under 120mÅ in the Sun and Arcturus. The EW values of lines in the Sun and Arcturus were measured from the high-quality spectra of Kurucz et al. (1984) and Hinkle et al. (2000), respectively, and are listed in Table 3. Table 3 contains a subjective quality assessment for each line, with A the highest quality and E the lowest.

In order to perform the differential abundance analysis it is necessary to adopt a microturbulent velocity value for the atmospheres of both stars. A sufficient approximation would be to choose a microturbulent velocity value for the Sun from the literature. However, we chose to estimate the microturbulent velocities for the Sun using an absolute abundance analysis, from a small sample of Fe I lines with accurate laboratory  $gf$ -values. We could then select the Arcturus microturbulent velocity by demanding that the differential abundances are independent of EW. Our adopted log  $gf$  values are unweighted averages from the work of three groups: O’Brian et al (1991); Bard et al. (1991) and Bard & Kock (1994); and Blackwell et al. (1992a,b, 1984, 1986, 1995). All three groups claim small uncertainties, near 0.04 dex, for most of their lines. Small systematic differences in the log  $gf$  values from the three sources indicate the values of the O’Brian group are systematically larger than the

Bard group and both groups have values larger than the Blackwell group; however the mean difference between the O’Brian and Blackwell groups, at only 0.03 dex, is comparable to the random uncertainties, and we have, therefore, chosen not to attempt systematic corrections of the  $\log gf$  scales. The adopted  $\log gf$  values and EWs in the Sun of these Fe I lines used for the absolute abundance analysis are listed in Table 4.

In the calculation of the abundances and microturbulent velocities we adopted solar atmosphere parameters of  $T_{\text{eff}}=5770$  K,  $\log g=4.44$ ,  $[m/H]=0.0$ , and Arcturus parameters of  $T_{\text{eff}}=4290$  K,  $\log g=1.55$ ,  $[m/H]=-0.50$ . The most appropriate models are the models including the new opacity distribution functions from Fiorella Castelli<sup>5</sup>, ODFNEW, for the solar model, and the alpha-element enhanced models with the new opacity distribution functions, AODFNEW, for Arcturus. With these models, and the best laboratory Fe I  $gf$  values listed in Table 4, we found microturbulent velocities for the Sun and Arcturus of 0.93 and 1.67 km/s, respectively. The absolute iron abundances, computed using the Fe I lines from Table 4 are 7.45 dex and 6.95 dex for the Sun and Arcturus respectively. Note that since the iron abundances of our stars are computed relative to Arcturus, they are not sensitive the absolute solar iron abundance.

We calculated the line-by-line differential iron abundance of Arcturus,  $[Fe/H]$ , relative to the Sun for a variety of model atmosphere grids. In the optimal case presented above, the line-by-line difference is  $-0.50$  ( $\sigma=0.07$ ). If ODFNEW models are used for both stars the difference is  $-0.56 \pm 0.07$ , while the difference is  $-0.51 \pm 0.07$  when AODFNEW models are used for both stars.

It is impressive that the  $[Fe/H]$  derived from Fe I lines is fairly insensitive to the choice of model atmosphere grid. In contrast, the iron abundance derived from Fe II lines is quite sensitive to the model atmosphere choice (for the three cases presented above the differences are  $-0.44 \pm 0.04$ ,  $-0.61 \pm 0.04$ ,  $-0.54 \pm 0.04$ , respectively) in a manner expected from the sensitivity of lines from ionized species to the electron pressure.

Although it would be possible to estimate  $\log gf$  values for our clean Fe lines in Table 3, we choose not to do so because of the strong dependence on the input assumptions, such as the model atmosphere grid used, the method for interpolation within the grid, and the spectrum synthesis program used for the analysis. Readers who wish to use this list of relatively unblended Fe-lines are advised to either perform a differential analysis themselves or to create astrophysical  $gf$ -values.

---

<sup>5</sup><http://wwwuser.oat.ts.astro.it/castelli/>.

## 5. Continuum and Line Measurements

Line measurements in very metal-rich giants require great care because of the difficulty of determining the continuum level in highly blanketed regions. For our highest resolution spectra of bulge giants, a 1% change in the continuum placement will yield a systematic 4.5 mÅ change in the equivalent width (EW) values. The effect of an additive shift to individual lines depends on the original line strength. A 4.5 mÅ increase of a hypothetical 120 mÅ line at 7000 Å increases the resulting abundance by about 0.02 dex, but the effect of the shift on the abundance determined from a 10 mÅ line is about 0.16 dex. The increased effect on weaker lines will affect the determination of the microturbulent velocity and excitation temperatures. Therefore we needed to employ a method to accurately determine the continuum level.

The spectra extracted by MAKEE, and IRAF scripts, were first roughly flattened by dividing by a blaze function spectrum. The blaze function was determined from fitting the continuum of a star with very few lines, typically a very metal-poor star, using the IRAF *continuum* script. Unfortunately, the blaze functions from the HIRES spectra were not very stable, and may have depended upon where in the sky the telescope was pointing; however, since several blaze function candidates were available, we chose the blaze function which gave the flattest normalized object spectrum. We note that the IRAF *continuum* fitting parameter variables are somewhat subjective in this method. For example, weak line blanketing, of order a few percent, if not accurately removed can introduce subtle ripples into the blaze function, that can create artificial high-points in the normalized spectrum.

Continuum fitting was performed using the semi-automated spectrum measuring program GETJOB (McWilliam et al. 1995b). Although GETJOB has options to automatically select continuum regions based on high points in the spectrum, we chose to use the mode where the continuum region wavelength bounds are given as inputs to the program. GETJOB would then fit the continuum fluxes, as a function of wavelength, using a polynomial least-squares fit. The order of the fit was automatically selected to minimize the chi-squared residual normalized by the number of degrees of freedom; typical fits were order 3 or 4 polynomials.

The input continuum regions were selected on the basis of spectrum synthesis experiments, including a spectrum synthesis of the very metal-rich red giant  $\mu$  Leo, over the 5000–8000 Å wavelength range. We used the same Kurucz line list, with added CN lines, used in the creation of the Fe line list discussed in section 4. The synthesized spectrum was then searched for regions where the normalized flux stayed above 0.99 for more than 0.3 Å (about 8 pixels in the HIRES spectra). These regions were then visually inspected in the observed  $\mu$  Leo spectrum to confirm that that synthesis accurately reflected the local

stellar spectrum and to ensure that no telluric or unidentified stellar lines were within that region. In the bluer regions, where the line blanketing is larger, we were forced to lower the threshold to 0.95, in order to have sufficient numbers of continuum regions per order. The list of continuum regions employed in this work are presented in Table 5. Table 5 also gives predicted relative flux values for these continuum regions in five stars: the Sun, Arcturus,  $\mu$  Leo, and the bulge giants I-025 and IV-003. These last two stars are respectively the most metal-rich and metal-poor stars in the bulge sample.

Prior to measuring line EWs in each star, we synthesized the flux for every continuum region using the Kurucz line list plus our CN list and an atmosphere with estimated stellar parameters (based on the photometric  $T_{\text{eff}}$ , see Section 6.1). The mean relative flux value within each continuum region was calculated and used as a correction factor within the GETJOB line measuring program. The GETJOB continuum fit would include a re-normalization for each continuum region, based on the predicted continuum line blanketing factor, in order to estimate the true continuum level. For the very metal-rich bulge giant I-025, the mean value of the 208 continuum regions is 0.994. During the interactive fitting process, the observed spectrum within each continuum region was visually compared to the synthesis to ensure that no telluric features had been velocity-shifted into the region.

With the continuum level set GETJOB automatically measured the EWs of the spectral lines, from least-squares Gaussian fits to the line profiles. GETJOB includes routines that search for line blends, based on the S/N of the spectrum. GETJOB also allows for fully interactive fits, where the user sets the pixel range over which the Gaussian fits are made; this interactive facility was used to check the EWs of all lines manually. The EW values for all lines, in all stars, of our bulge and solar neighborhood samples are presented in Table 6.

In Figure 3 we present an example of what can go wrong when mis-using an automated continuum algorithm that employs spectrum high points to set the continuum level. If the number of pixels summed is too small the continuum of metal-poor stars is set by statistical high points and peaks in the ripple of the blaze function, and other systematic errors. On the other hand, for very metal-rich stars the continuum regions are short and rare, so that the number of pixels summed is too large, and thus includes regions affected by line blanketing, resulting in underestimated continuum levels. Although these effects may result in continuum levels with typical errors of only a couple of percent, this size of error is enough to affect the derived line abundances, especially for weak lines, which are crucial to the determination of the microturbulent velocity.

Figure 3 shows that for photometric and ionization temperatures the systematic abundance errors, induced by continuum setting problems, ranging from +0.05 dex from metal-poor stars to  $-0.05$  dex for very metal-rich stars. The abundance differences are greater if

the temperature is set by Fe I excitation than for the ionization and photometric  $T_{\text{eff}}$  methods. This may be due to a correlation between line strength and the excitation potential of the line: weak lines, generally of higher excitation, are affected more by an additive offset from a continuum change. These lines will then be systematically lower or higher (depending on the direction of the continuum shift), affecting the slope of points on the excitation plot. Indeed, for the 11 stars in Figure 3 with  $[\text{Fe}/\text{H}] < -0.5$ , the excitation temperatures for the synthesis method are on average  $121 \pm 48$  K (standard deviation of the mean) cooler. This is enough to explain the lower abundances derived for the synthesis method measurements. Since ionization temperatures depend on the mean of many Fe lines rather than a slope, the effect is less sensitive to the weak lines, and so greatly diminished. Note that the change in abundances for ionization temperatures follows the same change seen in photometric temperatures, which means the changes in  $[\text{Fe}/\text{H}]$  seen is due to equivalent width and  $v_t$  changes.

## 6. Atmospheric Parameters

The high and variable extinction toward Baade’s Window (Stanek 1996; Frogel et al. 1999), and the possibility of variation in the ratio of total to selective extinction (Udalski 2003), increases the difficulty of determining stellar parameters of our bulge stars by purely photometric means. This is complicated by the lack of accurate distances for individual bulge stars. Given these uncertainties, and the potential for error in the abundances, we elect to calculate the stellar atmospheric temperatures using three independent methods: photometric color-temperature relations; temperatures based on the excitation of Fe I lines, with abundances taken relative to Arcturus; and temperatures based on ionization equilibrium of iron, again with abundances taken relative to Arcturus, and a gravity adopted from photometric data.

### 6.1. Choice of Atmosphere Model Grid

The use of an appropriate stellar atmosphere grid is important to high-quality abundance analysis. For example, in these stars, the continuous opacity is dominated by  $\text{H}^-$ . The formation of  $\text{H}^-$  depends greatly on the supply of free electrons contributed by metal atoms, especially Mg. Previous analyses (MR94, RM00, MR04, etc.) have found that bulge stars of all metallicities have enhanced Mg/Fe ratios as compared to the Sun, but not all of the other alpha-element ratios are similarly enhanced. Therefore, it is important to understand the effect of using either solar-ratio or alpha-enhanced model grids.

Similarly, there may be other assumptions (such as whether to use grids with overshooting on or off) that affect the final results. The primary analysis in this paper was done using Kurucz model grids<sup>6</sup> employing solar abundance ratios with overshooting turned on.

To determine how the assumptions of the different atmosphere grid types affects our abundance results we have repeated a subset of the abundance analyses with different atmosphere grids. In the investigation the line measurements and parameter-setting methods for the Arcturus and bulge star abundances remained unchanged; however, we note that the Arcturus analysis used in the line-by-line differential analysis is based on the same grid of atmospheres. We know that Arcturus is alpha-enhanced (Peterson et al. 1993; Fulbright, Rich & McWilliam 2005 in preparation), so the most appropriate model for an absolute abundance analysis is an alpha-enhanced model atmosphere. We note that our differential analysis, relative to Arcturus, roughly compensates for deficiencies in the models. This correction should be most accurate for stars having compositions and physical parameters similar to that of Arcturus.

The atmospheres included in the tests include Kurucz models with overshooting turned off (“NOVER” taken from the same Kurucz web site as the overshooting models), grids from Fiorella Castelli<sup>7</sup> using new opacity distribution functions assuming solar abundance ratios (“ODFNEW”) or alpha-enhanced abundance ratios (“AODFNEW”). Finally, we included “MARCS” models (Gustafsson et al. 1975) calculated by a binary executable file provided by M. Shetrone.

We present the results from the tests in Table 7. Each column of numbers gives the mean value of the difference of that parameter for the model grid in question minus the result from solar-ratio overshoot grid (our default grid). We calculated the mean difference for the entire sample and for a subsample of stars with  $[\text{Fe}/\text{H}] > 0$ . We tested the effect on the derived excitation and ionization  $T_{\text{eff}}$  values (see Section 6.4), the derived Fe I abundance for all three  $T_{\text{eff}}$  scales, and the ionization difference ( $\log \epsilon(\text{Fe II}) - \log \epsilon(\text{Fe I})$ ) for the photometric and excitation  $T_{\text{eff}}$  scales (the ionization  $T_{\text{eff}}$  scale is defined by forcing the ionization difference to zero). The value of  $\sigma$  given in the table is the standard deviation of the results.

The difference caused by the use of alpha-enhanced models was small: When photometric  $T_{\text{eff}}$  values were used, there was little change in the derived abundance from Fe I lines, but the ionization difference decreased by 0.03 dex—the abundance derived from Fe II lines is somewhat sensitive to increasing the alpha-abundance of the atmosphere. The effect is

---

<sup>6</sup><http://kurucz.harvard.edu/>

<sup>7</sup><http://wwwuser.oat.ts.astro.it/castelli/>.

larger in the more metal-rich stars ( $-0.07$  dex). It is not clear whether these alpha-enhanced models (where all of the alpha element abundances are increased by  $+0.4$  dex) are any more representative of the metal-rich bulge stars than the solar models. Previous analyses of metal-rich bulge stars have found enhanced Mg ratios, important to the supply of free electrons, and solar-ratio abundances of Si and Ca, which are important to the mean molecular weight of the atmosphere. It will probably be necessary to re-address this issue during the analysis of the alpha elements in a future paper.

As a warning, these tests do not show that solar-ratio or alpha-enhanced model grids are roughly interchangeable when applied to absolute abundance analyses, but only that a differential analysis can somewhat compensate for the use of atmosphere grids calculated with different input assumptions.

## 6.2. Photometric Data

All three methods used to derive the stellar model atmosphere parameters require some photometric inputs. One of the great improvements in observational data since the MR94 study is the availability of 2MASS JHK (Cutri et al. 2003) and OGLE VI (Szymanski et al. 1996) photometry for the bulge. Wozniak & Stanek (1996) and Stanek (1996) have also used the OGLE photometry to create a position-dependent reddening map for Baade’s Window, allowing for reddening estimates for each of our stars. The available OGLE data includes data for 25 of our 27 stars. For the two other stars (IV-047 and IV-167) TSR95 V magnitudes were used. Of our sample, only IV-047 does not have data in the 2MASS Point Source Catalog. It was necessary to transform the 2MASS data from the 2MASS filter system to the TCS filter system used by the Alonso et al. (1999) Teff-color relations using the transformations available on the 2MASS web site<sup>8</sup> and Alonso et al. (1998). Similarly, the reddening measures of Stanek (1996) were based on the SAAO filter system, so the  $E(B-V)$  measures were first transformed into the 2MASS system and removed from the data before any other transformations were applied. We list the final dereddened photometric data in Tables 1 and 2. We assume  $A_V = 3.136 E(B-V)$  from the reddening law of Winkler (1997). The final  $T_{\text{Phot}}$  values were calculated using Equation 9 of Alonso et al. (1999).

For the comparison disk sample, the V and B–V photometric data come from the Bright Star Catalog (Hoffleit & Warren 1991), while the V–K data is from Johnson et al. (1966) as found on SIMBAD. These stars are too bright for 2MASS to provide reliable photometry ( $\sigma_K \sim 0.3$  mag), so we were forced to adopt the  $T(B-V)$  when V–K data were not available.

---

<sup>8</sup><http://www.astro.caltech.edu/jmc/2mass/v3/transformations/>

Since all stars in the present disk sample were also studied by McWilliam (1990), we can use the McWilliam (1990) extinction estimates to correct the photometry: only HR 2113 was found to have any evidence for extinction, with  $A_V=0.17$  magnitudes. The  $T_{\text{Phot}}$  values derived for our 17 disk stars are on average  $50 \pm 29$  K cooler than the values derived in McWilliam (1990). The final photometric  $T_{\text{eff}}$  values are given in Table 7.

### 6.3. Distances and Surface Gravities

We can determine the surface gravity of a star if we know its mass ( $m$ ), temperature, and bolometric magnitude ( $M_{\text{bol},*}$ ) using the following well-known equation:

$$\log g = \log (m/m_{\odot}) - 0.4(M_{\text{Bol},\odot} - M_{\text{Bol},*}) + 4 \log (T/T_{\odot}) + \log g_{\odot} \quad (1)$$

We adopt  $M_{\text{Bol},\odot} = 4.72$ ,  $T_{\odot} = 5770$  K and  $\log g_{\odot} = 4.44$ . In the above equation, the uncertainty in  $\log g$  from distance errors scales roughly as 0.4 times the uncertainty in  $M_{\text{Bol},*}$  (which folds in errors in the bolometric correction, distance modulus, photometry, and reddening).

As stated before, there are no definitive distance determinations for any of our Baade’s Window sample stars. As discussed in Section 2, previous work shows that the individual probability that each star in our sample is a bulge member is very high. We can show that we do not need very accurate distances in order to determine good surface gravity values. We adopt a distance to the Galactic Center of 8.0 kpc, based on the work of Eisenhauer et al. (2003) and Reid (1993), which corresponds to a distance modulus of 14.51 mag. A  $\pm 0.5$  mag shift in the distance modulus changes the distance to either 6.3 or 10.0 kpc. In other words, a small distance modulus error quickly locates the star outside the bulge. A 0.5 mag error in  $M_{\text{Bol},*}$  leads to a 0.12 dex error in  $\log g$ , which has only a small effect (about 0.05 dex) on the final ionization equilibrium.

Therefore, we can assume with some certainty that all the bulge stars in our sample lie at a distance of  $8.0^{+2.0}_{-3.7}$  kpc. If the resulting abundances point to surface gravity selection problems (e.g., a large disagreement in the abundances derived from Fe I and Fe II), then it is very likely the star in question is not a bulge star.

For the disk sample only, we used the Hipparcos parallaxes (ESA 1997) to determine the distance to the stars. For most of these stars the parallax is known to better than 10%. The distances to the disk giants range from about 11 pc for Arcturus to about 145 pc for HR 1585.

### 6.4. Parameter Determination

The abundance analysis was conducted by a suite of programs customized to work with the MOOG equivalent width abundance analysis program. These programs applied the line-by-line differential analysis with respect to Arcturus and through an automatic iterative process would determine the best model atmosphere for the chosen method.

The main difference in the three parameter-setting methods is how the  $T_{\text{eff}}$  value is determined. The other major parameters ( $\log g$ ,  $[\text{m}/\text{H}]$ , and  $v_t$ ) are set in the same way in all three methods. Before we discuss the differences in the temperature-setting methods, we will discuss how the other three parameters are set.

As mentioned above, we determine the  $\log g$  value for all cases using Equation 1. For the Baade’s Window sample, we adopt a distance of 8 kpc and a stellar mass of  $0.8 M_{\odot}$ . For the disk sample, we use the Hipparcos distance and derive a mass by the location of the star in the  $M_{\text{Bol}}$  vs.  $\log T_{\text{eff}}$  diagram when compared to Padova evolutionary tracks (Girardi et al. 2000) of a similar metallicity. We assume  $M_{\text{Bol},\odot} = 4.72$ ,  $T_{\odot} = 5770$  K, and  $\log g_{\odot} = 4.44$ .

The bolometric corrections,  $\text{BC}(V)$ , for our stars come from Alonso et al. (1999). Our analysis program automatically recalculates new  $\text{BC}(V)$  and  $\log g$  values whenever either of the input variables ( $T_{\text{eff}}$  or  $[\text{Fe}/\text{H}]$ ) changes. If we adopt  $\text{BC}(K)$  instead of  $\text{BC}(V)$  the final  $M_{\text{Bol}}$  (see Section 7.2 and Table 8) is increased by  $+0.04 \pm 0.08$  mag; presumably this is the scale of the uncertainty of the bolometric corrections. Because the V-band suffers from greater line blanketing than the K-band in cool stars, we assume that  $\text{BC}(V)$  values are more sensitive to line formation; thus, we expect greater uncertainty in  $\text{BC}(V)$  for cool stars and stars with high metallicity or unusual composition. The difference between  $M(K)_{\text{Bol}}$  and  $M(V)_{\text{Bol}}$  for II-122 is  $-0.27$  mag. This star is closest to the RGB tip than any star in the Baade’s Window Sample. Use of  $M(K)_{\text{Bol}}$  instead of  $M(V)_{\text{Bol}}$  changes the final  $\log g$  value by only  $-0.11$  dex. There are only two other cases where the difference in bolometric magnitude exceeds 0.10 mag: two bright Baade’s Window giants (I-322 and IV-203), both with  $M_{\text{Bol}} < -2.25$ , show differences of  $+0.12$  and  $+0.11$  mag, respectively, between the  $M_{\text{Bol}}$  values derived from the K- and V-band. Therefore, it is likely the bolometric corrections become more uncertain with increasing luminosity, but the size of the uncertainty is not enough to cause major changes to the final abundances.

The microturbulence value ( $v_t$ ) was set by the slope of  $\log \epsilon(\text{Fe I})$  vs.  $\log(\text{RW})$  plot. The final  $v_t$  value was set by forcing the slope of a least-squares fit to the plot to be zero. The uncertainty in the final value can be estimated by the formula:

$$\sigma(v_t) = \sigma(\log \epsilon(\text{FeI})) \left( \frac{\delta(\log \epsilon(\text{Fe I}))}{\delta(v_t)} \right)^{-1} \quad (2)$$

where the  $\sigma(\log \epsilon(\text{FeI}))$  value is determined from the standard deviation of abundances of individual Fe I lines and  $\delta(\log \epsilon(\text{Fe I}))/\delta(v_t)$  is determined empirically by the analysis program. The atmospheric model  $[m/H]$  value was chosen to match the  $\log \epsilon(\text{Fe I})$  value determined by the previous iteration.

The “photometric temperature” ( $T_{\text{Phot}}$ ) method is the simplest. The final  $T_{\text{eff}}$  value is the one determined by the Alonso et al. (1999) (V–K)- $T_{\text{eff}}$  relationship. The main problem with this method is the possibility of uncorrected differential reddening. An error of 0.1 mag in E(B–V) will yield a change in  $T_{\text{eff}}$  of about 100 K in a 4000 K giant. The results from the  $T_{\text{Phot}}$  determinations were used as the initial conditions in the iterative method used to determine the excitation and ionization temperatures.

The availability of 2MASS colors means we could also derive photometric  $T_{\text{eff}}$  values from a (J–K)- $T_{\text{eff}}$  relationship. The use of two infrared bands reduces the sensitivity to reddening, but unfortunately the J–K color is not as sensitive to temperature changes as V–K. The Alonso et al. (1999) (J–K)- $T_{\text{eff}}$  relationship has an internal calibration uncertainty about five times larger than the (V–K)- $T_{\text{eff}}$  relationship (125K versus 25K). When applied to the Baade’s Window sample, the mean difference of  $T(\text{V–K}) - T(\text{J–K})$  is  $-19 \pm 113$  K (standard deviation). The quoted standard deviation of the difference is consistent with the uncertainty of  $T(\text{J–K})$  calibration.

The “excitation temperature” ( $T_{\text{Ex}}$ ) method requires that we adjust the  $T_{\text{eff}}$  value of the star until the slope of the  $\log \epsilon(\text{Fe I})$  vs. excitation potential (EP) plot is zero. This method (and the “ionization temperature” method below) reduces the potential problems due to reddening errors, but is not free from uncertainty. As mentioned earlier, in many of the stars the strong lines are also those with low EP and the weak lines are those with high EP. Our new line list reduces this problem somewhat, but in many stars the number of low excitation (EP < 3 eV) lines was small. Any problems with these lines could systematically cause errors in the  $T_{\text{eff}}$  values. We estimate the  $T_{\text{eff}}$  uncertainty by:

$$\sigma(\log T_{\text{Ex}}) = \sigma(\log \epsilon(\text{Fe I})) \left( \frac{\delta(\log \epsilon(\text{Fe I}))}{\delta(T_{\text{eff}})} \right)^{-1} \quad (3)$$

Finally, the “ionization temperature” ( $T_{\text{Ion}}$ ) method requires ionization equilibrium between Fe I and Fe II. Normally in spectroscopic parameter determinations the value of  $\log g$  is altered to force ionization equilibrium. In this method, the value of  $\log g$  is forced by the distance and mass (with a slight dependence on  $T_{\text{eff}}$ ) by Equation 1, so the main way to affect the ionization equilibrium is to change the  $T_{\text{eff}}$  value. A +100 K change in  $T_{\text{eff}}$  changes the value of  $\log \epsilon(\text{Fe II}) - \log \epsilon(\text{Fe I})$  by about  $-0.1$  dex.

The ionization temperatures method is insensitive to the effects of a few pathological

Fe I lines, but the scarcity of good Fe II lines is a concern, as any errors in the measurement and analysis of those lines could greatly affect the result. The sensitivity of the ionization equilibrium to  $\log g$  also means that distance errors could lead to large systematic errors in  $T_{\text{eff}}$  by this method. We estimate the internal  $T_{\text{eff}}$  uncertainty by:

$$\sigma(T_{\text{Ion}}) = \sigma(\Delta \log \epsilon(\text{Fe})) \left( \frac{\delta(\Delta \log \epsilon(\text{Fe}))}{\delta(T_{\text{eff}})} \right)^{-1} \quad (4)$$

where

$$\Delta \log \epsilon(\text{Fe}) = \log \epsilon(\text{Fe II}) - \log \epsilon(\text{Fe I}). \quad (5)$$

## 7. Results

### 7.1. Results of the Individual Methods

As described in the previous section, each of the three methods for determining the stellar temperatures have their own strengths and weaknesses. All three methods can give good results when the input data is accurate (as the results for the disk sample show below), so we have no initial preference for any of the methods. Our use of three methods for estimating  $T_{\text{eff}}$  ensures that our temperatures are robustly determined, and allows for us to check for systematic errors for individual measurements.

There are a few steps common to all three methods. Errors in those steps could lead all three methods to return incorrect results. For example, the effect of using different stellar atmosphere grids was discussed in Section 6.1. Our surface gravities rely on several inputs:  $T_{\text{eff}}$ , mass, and bolometric magnitude. The bolometric magnitude depends on the distance, photometric magnitude, and bolometric correction. Distance errors will have a large effect on the ionization  $T_{\text{eff}}$  values, and we discussed the effect of filter choice on the bolometric correction in Section 6.4.

If all three methods are valid and all the input data and assumptions are correct, the three  $T_{\text{eff}}$  values obtained should all agree and the stars should be in ionization and excitation equilibrium. In Figures 4 and 5, we plot the differences in  $T_{\text{eff}}$  determinations and between Fe I and Fe II abundances, respectively.

In both plots the disk stars show excellent agreement between all three  $T_{\text{eff}}$  methods. This shows that the methodology is sound when we know the star’s distance and reddening very well and the S/N level is very high. In addition, the disk star abundances agree with previous determinations. The mean [Fe I/H] for the 17 disk stars from this work are  $+0.07 \pm 0.02$  dex greater than found by McWilliam (1990) (for the 11 stars below solar

metallicity the mean difference is  $+0.03 \pm 0.02$  dex). The giants HR 1346 ( $\gamma$  Tau), HR 1409 ( $\epsilon$  Tau) and HR 1411 ( $\theta$  Tau) are all members of the Hyades cluster (vB 28, vB 70, and vB 71, respectively). The mean  $[\text{Fe}/\text{H}]$  value for the three stars is  $0.17 \pm 0.02$ . Boesgaard & Friel (1990) and Paulson et al. (2003) studied solar-type Hyades dwarfs (which avoids many of the analysis problems encountered here) and found a mean  $[\text{Fe}/\text{H}]$  values of  $+0.127 \pm 0.022$  and  $0.13 \pm 0.01$ , respectively. Given typical systematic abundance analysis scale uncertainties, of approximately 0.05 dex, we conclude that the abundances determined here are consistent with previous studies.

For the most part, the temperature values found for the bulge stars show excellent internal agreement as well. There are, however, six stars that do not show agreement in all of the various comparisons. The metallicity of these stars does not show any bias to high or low  $[\text{Fe}/\text{H}]$  values. Fortunately, we can diagnose the potential failures of the methods. For example, two of the six stars (IV-047 and II-172) show  $T_{\text{Phot}}$  values that are much lower than the  $T_{\text{Ex}}$  and  $T_{\text{Ion}}$  values, even though the later two are in agreement. The most likely source of the problem is poor photometry in the crowded field of Baade’s Window. For IV-047 there was no entry in the 2MASS Point Source Catalog, nor any other published JHK colors. Therefore, we were forced to use the photographic B–V colors of Arp (1965) and the  $T(\text{B–V})$  calibration of Alonso et al. (1999). The typical uncertainty in the Arp (1965) B–V colors of  $\sigma \sim 0.14$  magnitudes near  $V \sim 17$  (e.g. see van den Bergh 1971) corresponds to  $1\text{-}\sigma$   $T_{\text{eff}}$  uncertainty of  $\sim 200$  K; thus we give low weight to the photometric  $T_{\text{eff}}$  for IV-047.

The sample of SRT96 includes both II-172 and IV-047. They give V–I colors for both stars on the Cousins system. We use the color transformations of Bessell (1979) and  $E(\text{V–I})_{\text{C}} = 1.26 E(\text{B–V})$  to convert the colors onto the Johnson system for use in the color- $T_{\text{eff}}$  relations of Alonso et al. (1999). This yields  $T_{\text{eff}}$  values of 4393 K for II-172 and 4433 K for IV-047. Both of these values are much closer to the  $T_{\text{Ex}}$  and  $T_{\text{Ion}}$  values than the original  $T_{\text{Phot}}$  values.

For II-172, 2MASS data are available, but it is possible that crowding affected this star due to the relatively large pixels used in that survey. On the finding chart of Arp (1965), II-172 is located very close to a much brighter star; II-172 is the only star in our sample that suffers from this problem. The Alonso et al. (1999)  $T(\text{J–K})$  for II-172 is 4281 K, which is close to the  $T(\text{V–K})$  value of 4260 K. However, the  $T(\text{J–K})$  relation of Alonso et al. (1999) has an internal uncertainty five times larger than the  $T(\text{V–K})$  relation used here. Differential reddening is unlikely because the large  $T_{\text{eff}}$  difference ( $\sim 200$  K) would require a change of  $E(\text{B–V})$  of over 0.2 magnitudes.

A change in the distance modulus to either star would not solve the discrepancy. A 1 magnitude change in the distance modulus leads to a +65 K change in  $T_{\text{Ex}}$  and a –150 K

change in  $T_{\text{Ion}}$ . A distance change for these two stars could bring either  $T_{\text{Ion}}$  or  $T_{\text{Ex}}$  in agreement with  $T_{\text{Phot}}$ , but not both. Below we will use a distance change to correct cases where  $T_{\text{Ion}}$  is much different than  $T_{\text{Ex}}$  and  $T_{\text{Phot}}$ . Therefore, since we cannot find reliable  $T_{\text{Phot}}$  values for either IV-047 and II-172, we will ignore the  $T_{\text{Phot}}$  results for these two stars.

Another of the six “problem” stars is I-322. In this case, the  $T_{\text{Ex}}$  value is out of line with the other two methods. Under close inspection, the excitation plot of this metal-poor star contains only one line with an excitation potential of less than 1 eV. The least-squares fit is very sensitive to outliers, so it is possible that the real uncertainty of the  $T_{\text{Ex}}$  value is larger than the formal value of 37 K. No other simple solution would solve the problem, so we will ignore the  $T_{\text{Ex}}$  results for this star.

The star IV-203 probably isn’t a problem star at all. The spread in  $T_{\text{eff}}$  results is large, but that might be due to the increased line blanketing in this cool star. In this case, the standard deviation between the three  $T_{\text{eff}}$  method results is 59 K. This is larger than most of the other stars, but we believe this is not enough to merit any action.

For II-122 and IV-025 the initial analysis showed large differences in the ionization balance between Fe I and Fe II ( $\log \epsilon(\text{FeII}) - \log \epsilon(\text{FeI}) = +0.43$  for II-122 and  $-0.53$  for IV-025). The values of  $T_{\text{Phot}}$  and  $T_{\text{Ex}}$  show reasonable agreement, while  $T_{\text{Ion}}$  is forced to change greatly to bring the star into ionization equilibrium. The problem with these two stars is that we may have assumed the incorrect distance. Therefore, we adjust the distance modulus from 14.51 mag to minimize the ionization difference. For IV-025, we adjust  $M_V$  from +0.33 to +2.05, or to a new distance modulus of 12.78 ( $d = 3.6$  kpc), while for II-122 the  $M_V$  change was from  $-1.57$  to  $-2.92$  (a new distance modulus of 15.89,  $d = 15.1$  kpc). At these new distances, the ionization differences are reduced to less than 0.05 dex and the  $T_{\text{eff}}$  indicators agree to within about 120 K.

The need for a change in distance scale is further demonstrated in Figure 6. In Figure 6(a), we show the excitation plots ( $\log \epsilon(\text{Fe})$  vs. Excitation Potential) for the three methods for IV-025 assuming a distance of 8 kpc. For the photometric and excitation  $T_{\text{eff}}$  methods, the slope of the plot is very flat, but the Fe II abundances are much below the Fe I abundances. The  $T_{\text{eff}}$  change needed to bring the two species into agreement greatly affects the slope of the plot.

In Figure 6(b), we plot the same data except that the  $M_V$  value of IV-025 has been changed to the final value of +2.05. In all three panels the slope of the Fe I lines is flat and the mean abundance of the Fe II lines agree with the mean of the Fe I lines.

The new distances to these two stars places them outside the bulge. The low metallicity of II-122, at  $[\text{Fe}/\text{H}] = -0.79$ , and its distance, approximately 7 kpc beyond the bulge and

over 1 kpc away from the plane of the disk, suggests that it might reasonably be a member of the thick-disk or halo. Star IV-025 is metal-rich, at  $[\text{Fe}/\text{H}] = +0.21$ , but it is about 250 pc above the plane of the disk, roughly half way between the Sun and the bulge. We will continue to include these stars in our analysis, but will not include them in any future discussion of the bulge and its abundance properties.

## 7.2. Final Abundances

A summary of the  $T_{\text{eff}}$  and iron abundance results from the three methods is given in Table 8. The results for II-122 and IV-025 reflect the new assumed distances. Since most of the  $T_{\text{eff}}$  values given by the three methods are in very good agreement, we have decided to adopt the mean of the three (two in the case of IV-027, II-172 and I-322, as noted above) individual  $T_{\text{eff}}$  values as our final adopted  $T_{\text{eff}}$ . The analyses were re-run using these new  $T_{\text{eff}}$  values; the final parameters and abundance results are given in Table 9. In Table 9 and elsewhere, we use  $[m/\text{H}]$  to denote the scaled solar metallicity used in the stellar atmosphere model, and  $[\text{Fe}/\text{H}]$  to signify the iron abundance as derived from our analysis on our scale where the solar  $\log \epsilon(\text{Fe}) = 7.45$ .

## 7.3. Comparison to Previous Results

In Figure 7 we compare the  $[\text{Fe}/\text{H}]$  values derived in this paper (“ $[\text{Fe}/\text{H}]$  New”) against those derived by Rich (1988; R88), McWilliam & Rich (1994; MR94), Sadler, Rich & Terndrup (1996; SRT96) and McWilliam & Rich (2004; MR04). For the R88 data, we fit to the “Solution 1” values. We do the comparison against all stars that match between the samples, including the non-bulge stars II-122 and IV-025, but excluding any solar neighborhood stars shared in the samples (three stars in R88, two in MR94). In all four cases, the metallicities derived here are slightly lower than derived in previous works, especially at the metal-poor end. The mean differences between the common stars (in the sense of “old minus new”) are  $+0.34 \pm 0.18$  dex for the R88 sample,  $+0.04 \pm 0.17$  dex for the MR94 sample,  $+0.12 \pm 0.54$  dex for the SRT96 sample and  $+0.04 \pm 0.10$  dex for the MR04 sample.

The fits were performed using the “least-squares cubic” method of York (1966), which does not assume that the independent variables (here taken to be our new  $[\text{Fe}/\text{H}]$  values) are free of uncertainty. For the fits to the R88 sample, we use the  $\sigma[\text{Fe}/\text{H}]$  value given in their Table 11. That estimate is explicitly for their Solution 1, but we have used that value for all three solutions because no other values are available. For the SRT96 sample we use

their  $\sigma[\text{Fe}/\text{H}] = 0.24$  estimate. For the MR94, we use their  $\sigma[\text{Fe}/\text{H}]$  value. Finally, for the MR04 sample, we give both our and their  $[\text{Fe}/\text{H}]$  values equal weight since both analyses came from the same data:

$$[\text{Fe}/\text{H}]_{\text{R88}} = 0.907[\text{Fe}/\text{H}]_{\text{New}} + 0.311; \sigma = 0.173; r = 0.956; N = 21 \quad (6)$$

$$[\text{Fe}/\text{H}]_{\text{MR94}} = 0.802[\text{Fe}/\text{H}]_{\text{New}} - 0.025; \sigma = 0.131; r = 0.968; N = 11 \quad (7)$$

$$[\text{Fe}/\text{H}]_{\text{SRT96}} = 1.027[\text{Fe}/\text{H}]_{\text{New}} + 0.123; \sigma = 0.564; r = 0.669; N = 17 \quad (8)$$

$$[\text{Fe}/\text{H}]_{\text{MR04}} = 0.938[\text{Fe}/\text{H}]_{\text{New}} + 0.012; \sigma = 0.099; r = 0.989; N = 9 \quad (9)$$

The value of  $\sigma$  in the above equations indicates the formal root mean square scatter about each fit, and does not include the uncertainties on the individual  $[\text{Fe}/\text{H}]$  measurements from any of the works. The value of  $r$  is the correlation coefficient, and  $N$  is the number of stars matched between the two samples.

The solution for the SRT96 data includes two extreme outliers (III-220 and IV-047). Our calculated abundances for each star is over 1 dex different than what was derived by SRT96 (neither star in in R88). Such a difference could be due to mis-identifications by SRT96 or problems with their analysis procedure. SRT96 assigns very high metallicities ( $[\text{Fe}/\text{H}] > +1$ ) to some Baade’s Window giants, yet we do not confirm this result with our analysis. Three of our stars (I-025, I-039 and IV-047) were given  $[\text{Fe}/\text{H}]$  values larger than +0.8 by SRT96, but we find that all of them have  $[\text{Fe}/\text{H}] \leq +0.51$ . If the two extreme outliers are excluded from the comparison, the new fit becomes:

$$[\text{Fe}/\text{H}]_{\text{SRT96}} = 0.934[\text{Fe}/\text{H}]_{\text{New}} + 0.089; \sigma = 0.258; r = 0.906; N = 15. \quad (10)$$

We will use this second calibration between SRT96 and our results for the the derivation of the bulge metallicity distribution function in the next section. Note that the mean  $[\text{Fe}/\text{H}]$  difference between the 15 remaining common stars between the SRT96 and present sample becomes  $+0.11 \pm 0.25$  dex. The removal of the outliers barely changes the value of the mean but greatly reduces the size of the standard deviation.

#### 7.4. The Bulge Metallicity Distribution Function

The metallicity distribution function (MDF) is a powerful tool for understanding the star formation history within a population (Schmidt 1959; Searle & Sargent 1972). Rich (1990) measured the first MDF for the bulge and found that it was well fit by the classic closed box gas exhaustion model. This result means that the bulge does not suffer from the “G-dwarf” problem seen in the local disk. In practice, the wide abundance range was known since the 1950’s, as Baade and others knew that RR Lyrae stars (indicative of the old metal-poor population) and M-giants (indicative of the disk-like population) were present in the same field. This study confirms the presence of this wide abundance range.

While our sample size is not large enough to create an MDF from the high-resolution sample alone, we can use the fits derived above to recalibrate the larger low-resolution spectroscopic samples of R88 and SRT96 using the least-squares fits from the previous section. After recalibration, we calculate the value of the mass fraction of metals ( $Z$ ) assuming  $Z_{\odot} = 0.019$  and scaled solar element ratios. From MR94, RM00 and MR04, we know that certain  $\alpha$ -elements such as Mg are enhanced from solar, so the values of  $Z$  derived here are too low. It will be necessary to revisit the MDF once we have derived the abundances of other elements, especially the common heavy elements O, C, N, Mg, and Si.

Care has to be taken in selecting samples when calculating an MDF. In the case of the bulge, there is contamination by foreground and background stars. More importantly, very metal-rich giants quickly evolve into cool, strong-lined M-giants. Metallicity determination, either by high- or low-resolution methods, become very problematic in M-giants. Worse, near the boundary between K-giants and M-giants a slight increase in the  $[\text{Ti}/\text{Fe}]$  ratio could be enough to form the strong TiO bands characteristic of M-giants, but at higher  $T_{\text{eff}}$  than for solar neighborhood stars. This could create a sampling bias in which a K-giant sample under-estimates the frequency of stars with high  $[\text{Ti}/\text{Fe}]$  ratios.

Our metallicity recalibration is based on K-giants, so the most desirable situation is to use stars on a part of the giant branch where stars of all abundances are K-giants. Fortunately, SRT96 identified a subsample of 217 stars at and below the RGB clump that belong to the bulge population (196 clump stars and 21 bulge giants with  $V > 17$ ). These stars are warm enough ( $T_{\text{eff}} > 4000$ , as determined by SRT96) that even the coolest cannot have significant TiO formation. Many of these SRT96 stars (including stars we observed) have TiO band measures from R88. None of the SRT96 bulge clump stars that were observed in R88 have TiO band strength greater than the values observed in one or more of our recalibration stars. Thus, by using our sample of mostly clump stars to define the bulge MDF we count the stars without the metallicity and composition bias’ associated with stars that become M-giants. Since all bulge red giant stars go through the He-burning (HB) red clump it is an

excellent region to fully sample the MDF. We note that although the lifetimes of the helium burning phase is affected by metallicity, with a longer HB lifetime for more metal-rich stars, the size of the effect is relatively small: approximately 10% increase in HB lifetime for a 1 dex increase in metallicity (e.g. see Girardi et al. 2000; Cassisi et al. 2004). Our estimate of the correction to the MDF due to this effect, based on the tracks of Girardi et al. (2000), is similar to the uncertainty on the measured mean metallicity, with the corrected mean metallicity lower by  $\sim 0.02$ – $0.03$  dex.

An additional advantage of using clump stars is that the region of the color-magnitude diagram where they lie is dominated by bulge stars ( $P(\text{bulge}) > 80\%$ , as discussed in Section 2). Therefore, we have chosen to use only the 217 stars identified by SRT96 as bulge clump stars (out of the 268 stars they identify as bulge members) to define the bulge MDF. In a separate MDF estimate we will use the full sample of 88 stars from R88 because the initial star selection for that work focused on K-giants.

A final caveat: the recalibration performed here cannot correct for any selection bias or incompleteness in the initial samples. The reader should refer to the original papers for more detailed information. The advantage of our recalibration is that the high-resolution work, performed here, provides a way to correct for zero-point and scale errors of the SRT96 and R88 low-resolution metallicity scales.

In Figures 8 and 9 we plot the recalibrated MDF for the R88 and SRT96 data. Also plotted are closed-box gas exhaustion models (Rich 1990) using either the mean or median value of  $Z$  as the yield. Use of the median  $Z$  value in the model reduces the possibility that errors at either end of the recalibration offsets the final yield. The mean  $[\text{Fe}/\text{H}]$  values of the three samples are:  $-0.25 \pm 0.06$  (we quote the standard deviation of the mean for these mean values) for R88 Solution 1,  $-0.15 \pm 0.03$  for the 268 bulge stars in the full SRT96 sample,  $-0.10 \pm 0.04$  for the 217 clump plus faint bulge giants and  $-0.07 \pm 0.04$  for the 196 clump-only stars. The median values for these four samples are  $-0.20$  for the R88 sample, and  $-0.13$ ,  $-0.04$  and  $-0.01$  for the three SRT96 subsamples, respectively. If Equation 8 is used for the calibration of the SRT96 sample instead of Equation 10, the mean and median  $[\text{Fe}/\text{H}]$  for the 217 clump plus faint bulge giant stars become  $-0.12 \pm 0.03$  and  $-0.07$ .

The difference in the mean and median  $Z$  value for R88 is small compared to the scatter of the least-squares fit. The closed box model fits the R88 MDF well until approximately solar metallicity. The model under-predicts the number of stars with metallicities slightly greater than solar, then slightly over-predicts the number of very metal-rich stars.

Zoccali et al. (2003) gets a similar result for their fits to their MDF based on a  $M_K$  vs.  $(V-K)_0$  CMD of Baade’s Window. They admit that the calibration of the fiducial RGB

shapes they use are dependent on the observed abundances of the metal-rich globular clusters NGC 6528 and NGC 6553. They also find a sizable deficit of metal-poor stars ( $Z < 0.4 Z_{\odot}$ ) as compared to their model with a yield of solar metallicity.

The MDF from the recalibrated SRT96 clump star data shows a larger difference between the mean and median values of  $Z$  than the R88 sample, but this is reduced when compared to what is seen in the full-sample recalibration. For the full 268 star SRT96 recalibration, the mean  $Z$  value is  $1.36 Z_{\odot}$ , while the median  $Z$  is  $0.75 Z_{\odot}$ , as compared to 1.54 and  $0.91 Z_{\odot}$ , respectively, for the clump subsample. Both SRT96 samples contain many more super-solar metallicity stars than R88.

From Figure 9, it appears that a yield between the mean and median may be more appropriate. A higher yield fits the high-metallicity end of the distribution better, although it slightly under-predicts the number of metal-poor stars. A lower yield over-predicts the number of metal-poor stars and under-predicts the metal-rich end as well.

### 7.5. Bulge and Disk Metallicity Distribution Functions

In Figure 10 we plot the MDF from the corrected SRT96 clump sample to represent the bulge, and the MDF from Allende Prieto et al. (2004) to represent the disk. Allende Prieto et al. (2004) analyzed high-resolution spectra of the 104 stars within 15 pc of the sun. The internal errors of the Allende Prieto et al. (2004) data are much lower than the recalibrated SRT96 data, so we convolved the MDF with the uncertainty of the SRT96 data. This was done using by a summation of 104 Gaussians with  $\sigma = 0.283$  dex, each centered the  $[\text{Fe}/\text{H}]$  value of one of the stars in the Allende Prieto et al. (2004) sample. The summation was then binned and normalized.

The distribution of bulge stars is wider than the disk stars. For the Allende Prieto et al. (2004) MDF to have the same width as the bulge MDF, the width of the Gaussians used in the convolution above would have to be increased to about 0.45 dex, which is much larger than the measurement uncertainties of either work. The mean value of the raw disk sample is  $-0.13 \pm 0.03$  (standard deviation of the mean), or slightly below the mean of the SRT96 clump sample. Despite having a slightly higher mean value, the normalized bulge distribution has more very metal-poor stars than the disk sample (clear in the most metal-poor bin in the lower panel of Figure 10). We confirm R88: the “G-dwarf” problem, if it exists at all in the bulge, is less severe than in the local disk.

Solutions of the “G-dwarf” problem in the local disk include such theories as the infall of primordial gas (Larson 1974) or pre-enrichment of gas by an earlier star formation (Ostriker

& Thuan 1975). The lack of a “G-dwarf” problem in the bulge would limit the amount of infall or pre-enrichment needed to form the bulge. However, our sample size is small (only 12 stars with recalibrated  $[\text{Fe}/\text{H}]$  values below  $-1$ ; the closed-box model predicts 13.6 stars within this metallicity range), and complexities such as the shorter lifetimes of metal-poor HB stars and selection biases must be taken into consideration. If a number of these stars were not bulge members our conclusion could change. High resolution observations of all the metal-poor Baade’s Window stars would improve the derived metallicities and memberships of these stars.

Although the absence of a “G-dwarf” problem in the Galactic bulge complicates comparisons of its MDF with that of the disk, it is pertinent to ask how the bulge mean metallicity fits with the radial metallicity gradient seen in the Galactic disk (e.g. Janes 1979; Twarog et al. 1997). Given the mean  $[\text{Fe}/\text{H}] = -0.13$  dex for solar neighborhood stars within 15 pc of the Sun from Allende Prieto et al. (2004), and the best estimate of the radial  $[\text{Fe}/\text{H}]$  gradient, of  $-0.07$  dex per kpc, from Twarog et al. (1997), the mean  $[\text{Fe}/\text{H}]$  of the disk at the Galactic bulge is expected to be  $\sim +0.45$  dex. This value is significantly higher than our recalibration of the SRT96 dataset, with the mean  $[\text{Fe}/\text{H}] = -0.10 \pm 0.04$  dex; indeed the extrapolated mean disk value is roughly as high as the most metal-rich star in our sample of 27 bulge K giants. Although it is possible that the inner disk does have a mean metallicity of  $[\text{Fe}/\text{H}] \sim +0.45$  dex, with the bulge significantly lower, we favor the idea that, approximately within the solar circle, there is either no radial  $[\text{Fe}/\text{H}]$  gradient, or a very shallow gradient. This conclusion is the same as suggested by MR94 and Twarog et al. (1997); even Janes (1979) conceded the possibility of a zero gradient in the inner disk. The conclusion is based on the lack of a clear metallicity gradient in the range  $6.5 \leq R \leq 10$  kpc, and the absence of data for galactocentric radii less than  $R_G \sim 6$  kpc; outside  $R_G \sim 8-10$  kpc a strong metallicity gradient is clear in the extant data.

## 8. Summary

We have performed detailed abundance analysis of 27 K-giants in Baade’s Window, together with a control sample of 17 giants from the solar neighborhood. In this paper we focus on the stellar atmosphere parameters and iron abundances.

Because of the difficulties associated with the high interstellar extinction toward Baade’s Window we have employed three techniques to determine stellar effective temperature: photometric  $T_{\text{eff}}$ , based on  $V-K$  colors and the color-temperature calibration of Alonso et al. (1999); differential excitation temperatures, based on excitation equilibrium from Fe I lines; and differential ionization temperatures, based on ionization equilibrium of Fe I and Fe II

lines. The differential temperature estimates were taken relative to the bright K1.5 giant Arcturus, whose effective temperature is known to high accuracy. This differential technique offers the advantage that it is not limited by the paucity of Fe lines with accurate laboratory  $gf$ -values that are useful for analysis of red giant stars, and avoids the use of a disjoint collection of  $gf$ -values with a mixture of random and systematic uncertainties. Furthermore, with our differential abundances we expect some degree of canceling of abundance errors resulting from processes not included in the construction of the model atmosphere grid.

Our analysis of the 17 solar neighborhood giants confirms the consistency of the three methods used to estimate  $T_{\text{eff}}$  when reddening is negligibly small. Among the heavily reddened Baade’s Window stars these three techniques for temperature estimation have allowed us to identify two of our stars as non-bulge members.

In our abundance analyses we have included spectrum synthesis to identify lines blended with CN rotation-vibration lines, and random atomic features from the Kurucz database. In this way we have produced a list of iron lines that are clean in the metal-rich giant  $\mu$  Leo. Strengths of these iron lines are suitable for abundance analysis in both  $\mu$  Leo and Arcturus, which cover a range of  $\sim 0.8$  dex in metallicity.

We have also performed spectrum synthesis calculations to identify clean continuum regions in our stars. For heavily blanketed stars, where there are insufficient clean continuum regions, we estimated the blanketed flux in portions of the spectrum closest to the expected continuum. Typically we consider “dirty” continuum regions with less than 5% blanketing. Our syntheses provide us with flux corrections for these dirty continuum regions, to apply to the observed spectrum when making the continuum normalization. These continuum regions were especially important in the analysis of the metal-rich bulge stars, with the greatest line blanketing. We found that one result of misplaced continuum levels is large errors in the derived excitation temperatures.

Both the iron lines and continuum regions employed in this work are of general utility for the measurement of K-giant spectra with  $[\text{Fe}/\text{H}]$  values between about  $-1.5$  and  $+0.5$ .

The differential abundances of our bulge stars were put onto the solar scale by computing the differential abundances of our clean lines in Arcturus relative to the sun, based on EW measurements of those lines in the Kurucz et al. (1984) solar spectrum and the Hinkle et al. (2000) spectrum of Arcturus. In this way we find  $[\text{Fe}/\text{H}] = -0.50$  for Arcturus, with a scatter of 0.07 dex. The random error on the mean is less than 0.01 dex, but we believe that the total uncertainty is dominated by systematic effects, which we estimate may be  $\sim 0.05$  dex.

Our high-resolution iron abundance results agree closely with the values given for stars common to the samples of MR94 and MR04. The  $[\text{Fe}/\text{H}]$  values in our high-resolution sample

of bulge stars ranges from  $-1.29$  to  $+0.51$  dex, with a mean of  $-0.37$  dex; although the mean has no significance beyond a reflection of our sample selection biases. The mean differences between the common stars (in the sense of “old minus new”) are  $+0.34 \pm 0.18$  dex for the R88 sample,  $+0.04 \pm 0.17$  dex for the MR94 sample,  $+0.12 \pm 0.54$  dex for the SRT96 sample and  $+0.04 \pm 0.10$  dex for the MR04 sample.

In order to estimate the bulge metallicity distribution function we have corrected the results of R88 and SRT96, which were based on low-resolution spectra, onto our system by transformation equations based on stars in common with the current investigation.

For the transformed R88 sample (Solution 1) we obtain a mean  $[\text{Fe}/\text{H}] = -0.25 \pm 0.06$  dex, consistent with the re-calibration of the R88 work by MR94. For the re-calibrated full sample of SRT96 we obtain a mean  $[\text{Fe}/\text{H}] = -0.15 \pm 0.03$  dex.

The stars studied here and in SRT96 and R88, were restricted to K-giant stars, and thus give a biased metallicity distribution function. To avoid this bias we have selected SRT96 stars identified by them as members of the bulge red clump. Because all red giant stars in the bulge pass through the red clump phase, the red clump stars offer the potential for the most reliable estimate of the true bulge metallicity function for giant stars. We estimate that a small bias, due to slightly longer lifetimes for metal-rich red clump stars than the metal-poor variety requires a decrease of approximately 0.02 to 0.03 dex in the mean  $[\text{Fe}/\text{H}]$  of the metallicity distribution function. Thus, our best estimate for the mean  $[\text{Fe}/\text{H}]$  of the Galactic bulge is  $-0.10 \pm 0.04$  dex, based on our high-resolution re-calibration of the SRT96 results.

Our re-calibration of the SRT96 data, together with abundance results for solar neighborhood stars by Allende Prieto et al. (2004), confirms the conclusion, first made by Rich (1990), that the G-dwarf problem (i.e. a deficit of metal-poor stars relative to the Simple chemical evolution model) is either non-existent in the bulge, or much less severe than in the solar neighborhood.

Although the bulge and inner disk are two separate systems we note that the mean bulge  $[\text{Fe}/\text{H}]$  measured here, at  $-0.10$  dex, lies far below the extrapolated mean  $[\text{Fe}/\text{H}]$  value for the inner Galactic disk, at  $\sim +0.45$  dex, based on a linear Galactic radial metallicity gradient of  $-0.07$  dex per kpc (e.g. Twarog et al. 1997). Instead, we favor the idea of a zero, or much reduced, radial metallicity gradient in the Galactic disk, for  $R_G$  within the solar circle, as discussed by MR94.

We are especially grateful to the staff of Keck Observatory for their assistance, and S. Vogt and his team for building HIRES. The authors would like to thank Ruth Peterson

for many useful suggestions in the referee report. We acknowledge support from grant AST-0098612 from the National Science Foundation. For the Arcturus abundance analysis we gratefully acknowledge partial support from a NASA-SIM Key Project grant, entitled “*Anchoring the Population II Distance Scale: Accurate Ages for Globular Clusters and Field Halo Stars*”. The authors acknowledge the cultural role that the summit of Mauna Kea has had within the indigenous Hawaiian community. We are fortunate to have the opportunity to conduct observations from this mountain. This publication makes use of data products from the Two Micron All Sky Survey, which is a joint project of the University of Massachusetts and the Infrared Processing and Analysis Center/California Institute of Technology, funded by the National Aeronautics and Space Administration and the National Science Foundation. This research has also made use of the SIMBAD database, operated at CDS, Strasbourg, France.

## REFERENCES

- Allende Prieto, C., Barklem, P. S., Lambert, D. L. & Cunha, K. 2004, *A&A*, 420, 183
- Alonso, A., Arribas, S. & Martinez-Roger, C. 1998, *A&AS* 131, 209
- Alonso, A., Arribas, S. & Martinez-Roger, C. 1999, *A&AS* 140, 261
- Alonso, A., Salaris, M., Arribas, S., Martinez-Roger, C., & Asensio Ramos, A. 2000, *A&A*, 355, 1060
- Arp, H. 1965, *ApJ*, 141,43
- Asplund, M., Nordlund, Å., Trampedach, R. & Stein, R. F. 2000, *A&A*, 359, 743
- Asplund, M., Grevesse, N. & Sauval, A. J. 2004, *astro-ph/04010214*
- Augason, G.C., Taylor, B.J., Strecker, D.W., Erickson, E.F., & Witteborn, F.C. 1980, *ApJ*, 235, 138
- Ayres, T.R., & Linsky, J.L. 1975, *ApJ*, 200, 660
- Bard, A., & Kock, M. 1994, *A&A*, 282, 1014
- Bard, A., Kock, A., & Kock, M. 1991, *A&A*, 248, 315
- Bell, R.A., & Gustafsson, B. 1989, *MNRAS*, 236, 653
- Bessell, M. S. 1979, *PASP*, 91, 589

- Blackwell, D.E., Booth, A.J., Haddock, D.J., Petford, A.D., & Leggett, S.K. 1986, MNRAS, 220, 549
- Blackwell, D.E., Booth, A.J., & Petford, A.D. 1984, A&A, 132, 236
- Blackwell, D. E., Booth, A. J., Petford, A. D. & Laming, J. M. 1989, MNRAS, 236, 235
- Blackwell, D.E., Lynas-Gray, A.E., & Smith, G. 1995, A&A, 296, 217
- Blackwell, D. E., Petford, A. D., Arribas, S., Haddock, D.J. & Selby, S. J. 1990, A&A, 232, 396
- Blackwell, D.E., Petford, A.D., Shallis, M.J., & Simmons, G.J. 1982a, MNRAS, 199, 43
- Blackwell, D.E., Petford, A.D., & Simmons, G.J. 1982b, MNRAS, 201, 595
- Boesgaard, A. M. & Friel, E. D. 1990, ApJ, 351, 467
- Carney, B.W., Fulbright, J.P., Terndrup, D.M., Suntzeff, N.B., & Walker, A.R. 1995, AJ, 110, 1674
- Cassisi, S., Castellani, M., Caputo, F., & Castellani, V. 2004, A&A, 426, 641
- Castro, S., Rich, R.M., McWilliam, A., Ho, L.C., Spinrad, H, Filippenko, A.V., & Bell, R.A. 1996, AJ, 111, 2439
- Cutri, R. M., et al. 2003, 2MASS All-Sky Catalog of Point Sources, VizieR, II/246
- Eisenhauer, F., Schdel, R., Genzel, R., Ott, T., Tecza, M., Abuter, R., Eckart, A. & Alexander, T. 2003, ApJ, 597, L121
- Elmegreen, B. G. 1999, ApJ, 517, 103
- ESA 1997, The Hipparcos and Tycho Catalogues (ESA SP-1200) (Noordwijk: ESA)
- Frogel, J.A., Tiede, G.P., & Kuchinski, L.E. 1999, AJ, 117, 2296
- Fulbright, J. P. 2000, AJ, 120, 1841
- Girardi, L., Bressan, A., Bertelli, G. & Chiosi, C. 2000, A&AS 141, 371
- Grevesse N. & Sauval A.J., 1998, in: Frlich C., Huber M.C.E., Solanki S.K., et al., ed. Solar composition and its evolution—from core to corona. Dordrecht: Kluwer, p. 161
- Griffin, R. E. M. & Lynas-Gray, A. E. 1999, AJ, 117, 2998

- Gustafsson, B., Bell, R. A., Eriksson, K. Nordlund, A. 1975, *A&A*, 42, 407
- Hinkle, K., Wallace, L., Valenti, J., & Harmer, D., eds. 2000, *Visible and Near Infrared Atlas of the Arcturus Spectrum 3727–9300 Å* (San Francisco: ASP)
- Hoffleit, D. & Warren, Jr., W. H. 1991, *Yale Bright Star Catalog, Fifth Edition* (New Haven: Yale Univ. Obs.)
- Janes, K.A. 1979, *ApJS*, 39, 135
- Johnson, H. L., Iriarte, B., Mitchell, R. I. & Wisniewski, W. Z. 1966, *Comm. Lunar Plan. Lab.*, 4, 99
- Kauffmann, G. 1996, *MNRAS*, 281, 487
- Kurucz, R.L., Furenlid, I., & Brault, J. 1984, in *National Solar Observatory Atlas, vol. 1, Solar Flux Atlas from 296 to 1300 nm* (Sunspot: NSO)
- Kurucz, R.L. 1993, *IAU Commission 43, Ed. E.F.Milone*, p.93
- Lambert, D.L., & Ries, L.M. 1981, *ApJ*, 248, 228
- Larson, R. B. 1974, *MNRAS*, 166, 585
- Matteucci, F., Romano, D. & Molaro, P. 1999, *A&A*, 95, 828
- McWilliam, A. 1990, *ApJS*, 74, 1075
- McWilliam, A., & Rich, R.M. 1994, *ApJS*, 91, 749 (MR94)
- McWilliam, A., Preston, G.W., Sneden, C., & Searle, L. 1995, *AJ*, 109, 2757
- McWilliam, A., Preston, G.W., Sneden, C., & Searle, L. 1995, *AJ*, 109, 2736
- McWilliam, A. 1997, *ARA&A*, 35, 503
- McWilliam, A., & Rich, R.M. 2004, in *Origin and Evolution of the Elements*, ed. A. McWilliam & M. Rauch, *Carnegie Observatories: Pasadena*, (<http://www.ociw.edu/ociw/symposia/series/symposium4/proceedings.html>)
- McWilliam, A., in progress.
- Merrifield, M.R. 1992, *AJ*, 103, 1552
- O’Brian, T. R., Wickliffe, M. E., Lawler, J. E. Whaling, W. & Brault, J. W. 1991, *J. Opt. Soc. Am. B*, 8, 1185

- Ostriker, J. P. & Thuan, T. X. 1975, ApJ, 202, 353
- Paulson, D. B., Sneden, C. & Cochran, W. D. 2003, AJ, 125, 3185
- Perrin, G., Coudé du Foresto, V., Ridgway, S.T., Mariotto, J.-M., Traub, W.A. et al. 1998, A&A, 331, 619
- Peterson, R. C., Dalle Ore, C. M. & Kurucz, R. L. 1993, ApJ, 404, 333
- Quirrenbach, A., Mozurkewich, D., Buscher, D.F., Hummel, C.A., & Armstrong, J.T. 1996, A&A, 312, 160
- Reid, M. J. 1993, ARA&A, 31, 345
- Rich, R.M. 1988, AJ, 95, 828 (R88)
- Rich, R.M. 1990, ApJ, 362, 604
- Rich, R.M., & McWilliam, A. 2000, SPIE, 4005, 150 (RM00)
- Sadler, E. M., Rich, R. M. & Terndrup, D. M. 1996, AJ, 112, 171
- Schmidt, M. 1959, ApJ, 129, 243
- Searle, L. & Sargent, W. L. W. 1972, ApJ, 172, 25
- Smecker-Hane, T.A., & McWilliam, A. 2004, ApJ *submitted* (astro-ph/0205411)
- Sneden, C. 1973, ApJ, 184, 839
- Stanek, K.Z. 1996, ApJ, 460, L37
- Szymanski, M., Udalski, A., Kubiak, M., Kaluzny, J., Mateo, M. & Krzeminski, W. 1996, AcA, 46, 1
- Tinsley, B. M. 1979, ApJ, 229, 1046
- Timmes, F. X., Woosley, S. E. & Weaver, T. A. 1995, ApJS, 98, 617
- Twarog, B.A., Ashman, K.M., & Twarog, B.J. 1997, AJ, 114, 2556
- Udalski, A. 2003, ApJ, 590, 284
- van den Bergh, S. 1971, AJ, 76, 1082
- Vogt, S. S. 1987, PASP, 99, 1214

- Vogt, S. S. et al. 1994, SPIE, 2198, 362
- Wheeler, J. C., Sneden, C. & Truran, J. W. 1989, ARA&A, 27, 279
- Whitford, A.E., & Rich, R.M. 1983, ApJ, 274, 723
- Winkler, H. 1997, MNRAS, 287, 481
- Woosley, S.E., & Weaver, T.A. 1995, ApJS, 101, 181
- Wozniak, P. R. & Stanek, K. Z. 1996, ApJ, 464, 233
- Wyse, R. F. G., Gilmore, G. & Franx, M. 1997, ARA&A, 35, 637.
- York, D. 1966, Can. J. of Phys., 44, 1079
- Zoccali, M., Renzini, A., Ortolani, S., Greggio, L., Saviane, I., Cassisi, S., Rejkuba, M.,  
Barbuy, B., Rich, R. M. & Bica, E. 2003, A&A, 399, 931

Table 1. Keck/HIRES Journal of Observations

Name	$V_{\circ}$	$(V-K)_{\circ}$	Date	Slit <sup>a</sup>	Exp. (s)	Coverage (Å)	S/N per pixel <sup>b</sup>	E(B–V) (mag)
I-012	14.37	2.929	2000-07-04	C1	6000	5425–7750	90	0.430
I-025	15.42	2.864	2000-07-03	B2	8000	5425–7750	45	0.427
I-039	15.59	2.723	1998-08-16	C1	6000	5475–7825	55	0.414
I-141	14.55	2.907	2001-07-16	B2	6000	5500–7900	75	0.420
I-151	14.47	2.708	2001-08-14	C1	6000	5500–7900	60	0.423
I-152	15.42	2.431	2001-08-14	C1	6000	5500–7900	45	0.423
I-156	14.75	2.908	2001-08-14	C1	6000	5500–7900	60	0.423
I-158	15.15	2.828	2001-08-14	C1	6000	5500–7900	55	0.423
I-194	14.77	3.134	1998-08-15	C1	8000	5500–7825	75	0.426
I-202	14.46	3.050	1999-09-01	C1	7500	5425–7875	70	0.426
I-264	12.97	3.269	2000-08-01	C1	1800	5375–7750	85	0.447
I-322	13.01	3.131	1999-09-09	C1	4500	5425–7875	130	0.463
II-033	13.97	2.890	2000-08-01	C1	3600	5375–7750	75	0.477
II-119	14.14	2.552	2000-08-01	C1	3600	5375–7750	60	0.488
II-122	12.98	3.769	2001-06-28	C1	4000	5475–7750	80	0.502
II-154	14.97	2.440	2000-08-02	C1	6300	5375–7750	55	0.500
II-172	15.46	2.958	2000-08-02	C1	7500	5375–7900	55	0.490
III-152	14.64	3.124	1999-08-18	C1	4500	5500–7875	85	0.438
III-220	14.97	2.571	2001-07-16	C1	6000	5425–7875	60	0.515
IV-003	13.70	2.711	1999-07-19	C1	4500	5425–7875	80	0.439
IV-025	14.84	2.419	1999-07-18	C1	8000	5500–7875	40	0.438
IV-047	15.68	1.07 <sup>c</sup>	2000-07-03	B2	6000	5425–7750	40	0.414
IV-072	14.93	2.984	1998-08-14	C1	14000	5425–7850	100	0.428
IV-167	15.59	2.946	1999-07-19	B2	10000	5425–7875	75	0.450
IV-203	12.52	3.776	1999-09-11	C1	1440	5425–7875	70	0.435
IV-325	15.58	2.958	2000-08-01	C1	3600	5350–7875	70	0.414
IV-329	13.81	3.103	2000-04-20	C1	4200	5425–7850	90	0.414
$\mu$ Leo	3.88	2.66	2000-07-04	B2	2	5425–7750	220	0.000

<sup>a</sup>Slit C1 is 0.861 arcsec by 7 arcsec and yields an instrumental resolution of 45000, while slit B2 is 0.571 arcsec by 7 arcsec and yields a resolution of 60000.

<sup>b</sup>Peak value in the order containing H $\alpha$ .

<sup>c</sup>Value given for IV-047 is (B–V) $_{\circ}$  based on Arp (1965) photometry. The  $V_{\circ}$  is based on TSR95 data.

Table 2. Las Campanas/Lick Journal of Observations<sup>a</sup>

Name	$V_{\circ}$	$(B-V)_{\circ}$	$(V-K)_{\circ}$	Date	Exp. (sec)	S/N per pixel
HR1184 $\rho$ For	5.54	0.98	...	2003-12-31	15	175
HR1346 $\gamma$ Tau	3.65	0.98	2.14	2003-12-31	3	175
HR1348 $\phi$ Tau	4.96	1.15	...	2003-12-31	10	200
HR1409 $\epsilon$ Tau	3.54	1.03	2.21	2003-12-31	3	175
HR1411 $\theta$ Tau	3.85	0.95	2.10	2003-12-31	3	140
HR1585	5.50	1.31	...	2003-12-31	10	150
HR2035 $\delta$ Lep	3.81	0.99	2.54	2004-01-02	3	200
HR2113 <sup>b</sup>	4.37	1.17	2.83	2004-01-06	5	220
HR2443 $\nu$ Cma	4.43	1.15	2.61	2004-01-06	5	210
HR3418 $\sigma$ Hya	4.45	1.22	2.64	2004-01-06	5	210
HR3733 $\lambda$ Pyx	4.73	0.91	2.05	2003-12-31	5	190
HR4104 $\alpha$ Ant	4.28	1.45	3.41	2003-12-31	5	270
HR4382 $\delta$ Crt	3.56	1.11	2.61	2004-01-05	5	325
HR4450 $\xi$ Hya	3.54	0.96	2.09	2004-01-01	5	110
HR4608 $o$ Vir	4.13	0.97	2.22	2004-01-03	5	240
HR5340 $\alpha$ Boo	-0.04	1.23	3.00	1997-05-13	10	220

<sup>a</sup>All of the above observations were taken with the echelle spectrograph on the du Pont 2.5-m telescope at Las Campanas Observatory with the exception of HR5340 ( $\alpha$  Boo). The spectrum of  $\alpha$  Boo was taken with the 0.6-m CAT telescope at Lick Observatory and the Hamilton spectrograph. See the text for more details.

<sup>b</sup>Assumes  $A_V = 0.17$  from McWilliam (1990).

Table 7. Mean Effects from Changing Atmosphere Grids<sup>a</sup>

Atm. Grid	$\Delta T_{\text{Ex}}$	$\Delta T_{\text{Ion}}$	$\Delta \epsilon(\text{Fe I})_{\text{Phot}}^{\text{b}}$	$\Delta(\text{II-I})_{\text{Ex}}^{\text{c}}$	$\Delta \epsilon(\text{Fe I})_{\text{Ex}}$	$\Delta(\text{I-II})_{\text{Ex}}$	$\Delta \epsilon(\text{Fe I})_{\text{Ion}}$
ALL STARS							
ODFNEW	-2	-15	-0.01	-0.02	+0.00	-0.01	-0.01
$\sigma$	+11	+21	+0.02	+0.03	+0.02	+0.02	+0.02
AODFNEW	-3	-26	-0.01	-0.03	+0.00	-0.02	+0.00
$\sigma$	+24	+30	+0.02	+0.03	+0.01	+0.02	+0.01
NOVER	+3	-8	-0.01	-0.01	+0.00	+0.01	-0.01
$\sigma$	+22	+12	+0.01	+0.01	+0.04	+0.06	+0.01
MARCS	+3	+1	+0.00	+0.01	+0.01	+0.07	+0.00
$\sigma$	16	+26	+0.01	+0.04	+0.02	+0.10	+0.02
STARS WITH $[\text{Fe}/\text{H}] > 0$							
ODFNEW	-12	-38	-0.03	-0.04	-0.02	-0.02	-0.03
$\sigma$	+14	+12	+0.02	+0.03	+0.02	+0.02	+0.01
AODFNEW	-26	-59	-0.01	-0.07	+0.01	-0.02	+0.00
$\sigma$	+24	+17	+0.01	+0.02	+0.01	+0.02	+0.01
NOVER	+3	-13	+0.00	-0.01	+0.00	-0.01	+0.00
$\sigma$	+7	+8	+0.01	+0.01	+0.01	+0.02	+0.01
MARCS	+22	+28	+0.01	+0.04	+0.02	+0.08	+0.01
$\sigma$	13	+23	+0.01	+0.03	+0.01	+0.04	+0.02

<sup>a</sup>Differences defined as the result from the listed atmosphere minus the result from the default Kurucz atmosphere (solar abundance ratios with overshoot).

<sup>b</sup>For shorthand, we will use  $\epsilon$  instead of  $\log \epsilon$  in table headers.

<sup>c</sup>The ionization difference is defined as the value of  $\log \epsilon(\text{FeII}) - \log \epsilon(\text{FeI})$ .

Table 8. Parameter Determinations

Name	$M_V$	Mass	$T_{\text{Phot}}$	$\epsilon(\text{FeI})$	$\Delta(\text{II-I})$	$T_{\text{Ex}}$	$\epsilon(\text{FeI})$	$\Delta(\text{II-I})$	$T_{\text{Ion}}$	$\epsilon(\text{FeI})$	$\langle T \rangle$	$\sigma T$
BAADE'S WINDOW BULGE STARS												
I-012	-0.14	0.8	4278	7.08	+0.04	4204	7.06	+0.09	4289	7.08	4257	46
I-025	+0.90	0.8	4331	7.97	+0.05	4324	7.96	+0.05	4364	7.95	4340	21
I-039	+1.09	0.8	4430	7.96	-0.09	4371	7.94	-0.03	4356	7.93	4386	39
I-141	+0.04	0.8	4293	7.17	+0.08	4376	7.18	-0.03	4336	7.17	4335	42
I-151	-0.04	0.8	4434	6.69	-0.03	4402	6.67	-0.01	4379	6.65	4405	28
I-152	+0.91	0.8	4666	7.45	-0.03	4609	7.43	+0.04	4664	7.45	4646	32
I-156	+0.24	0.8	4292	6.74	+0.04	4323	6.74	-0.01	4320	6.75	4312	17
I-158	+0.64	0.8	4347	7.25	-0.04	4368	7.24	-0.08	4333	7.24	4349	18
I-194	+0.26	0.8	4153	7.20	0.00	4218	7.20	-0.10	4157	7.19	4176	36
I-202	-0.05	0.8	4204	7.61	-0.05	4184	7.59	-0.08	4163	7.60	4184	21
I-264	-1.54	0.8	4081	6.29	+0.05	4103	6.29	-0.01	4108	6.29	4097	14
I-322	-1.50	0.8	4155	7.20	-0.13	4293	7.23	-0.37	4058	7.20	4106	69
II-033	-0.54	0.8	4304	6.71	-0.04	4279	6.70	-0.01	4247	6.68	4277	29
II-119	-0.37	0.8	4563	6.24	-0.04	4605	6.28	-0.10	4493	6.18	4554	57
II-154	+0.46	0.8	4657	6.85	-0.02	4662	6.85	-0.02	4630	6.83	4650	17
II-172	+0.95	0.8	4260	7.11	+0.33	4447	7.14	+0.10	4514	7.16	4480	47
III-152	+0.13	0.8	4158	7.04	0.00	4165	7.03	-0.02	4149	7.02	4157	8
III-220	+0.46	0.8	4543	7.13	-0.01	4565	7.14	-0.03	4542	7.13	4550	13
IV-003	-0.80	0.8	4438	6.17	-0.01	4429	6.15	+0.02	4433	6.16	4433	5
IV-047	+1.17	0.8	4250	6.97	+0.44	4530	7.03	+0.05	4581	7.06	4556	36
IV-072	+0.42	0.8	4250	7.71	+0.05	4300	7.68	-0.06	4266	7.68	4272	26
IV-167	+1.08	0.8	4275	7.91	+0.06	4315	7.90	-0.01	4312	7.90	4301	22
IV-203	-2.00	0.8	3856	6.15	+0.23	3882	6.15	+0.17	3969	6.16	3902	59
IV-325	+1.07	0.8	4267	7.72	+0.07	4288	7.70	+0.01	4312	7.71	4289	23
IV-329	-0.70	0.8	4171	6.50	+0.08	4205	6.50	+0.01	4216	6.51	4197	23
BAADE'S WINDOW NON-BULGE STARS												
II-122 <sup>a</sup>	-2.92	0.8	3856	6.66	+0.13	3973	6.66	-0.07	3907	6.64	3919	59

Table 8—Continued

Name	$M_V$	Mass	$T_{\text{Phot}}$	$\epsilon(\text{FeI})$	$\Delta(\text{II-I})$	$T_{\text{Ex}}$	$\epsilon(\text{FeI})$	$\Delta(\text{II-I})$	$T_{\text{Ion}}$	$\epsilon(\text{FeI})$	$\langle T \rangle$	$\sigma T$
IV-025 <sup>b</sup>	+2.05	0.8	4682	7.68	-0.10	4557	7.66	+0.03	4599	7.66	4514	66
LOCAL DISK STARS												
HR1184	+0.85	0.9	4765	7.07	-0.02	4750	7.07	-0.01	4743	7.06	4753	11
HR1346	+0.28	1.9	4877	7.63	-0.07	4814	7.59	-0.05	4779	7.57	4823	50
HR1348	-0.14	1.6	4452	7.10	-0.04	4364	7.07	+0.06	4412	7.08	4409	44
HR1409	+0.16	2.6	4863	7.66	+0.02	4781	7.62	+0.10	4869	7.66	4838	49
HR1411	+0.43	2.6	5013	7.65	-0.02	4891	7.59	+0.11	4979	7.64	4961	63
HR1585	-0.31	1.0	4324	7.11	-0.03	4376	7.13	-0.08	4299	7.11	4333	39
HR2035	+1.13	0.9	4661	6.83	-0.04	4595	6.79	+0.02	4617	6.80	4624	34
HR2113	-1.18	1.3	4323	6.83	-0.14	4277	6.81	-0.09	4230	6.79	4277	46
HR2443	-1.34	1.6	4432	7.24	-0.05	4460	7.25	-0.10	4395	7.22	4429	33
HR3418	-0.72	2.2	4490	7.62	+0.04	4393	7.58	+0.15	4528	7.62	4470	70
HR3733	+1.00	2.3	5040	7.36	+0.04	4945	7.29	+0.09	5017	7.33	5001	50
HR3905	+0.83	1.3	4525	7.78	+0.04	4523	7.77	+0.03	4546	7.78	4531	13
HR4104	-0.97	0.8	4045	7.09	+0.04	4057	7.06	-0.05	4037	7.05	4046	10
HR4382	-0.32	1.0	4527	6.94	-0.04	4393	6.87	+0.12	4506	6.93	4475	72
HR4450	+0.55	1.6	5011	7.60	-0.07	4996	7.59	-0.06	4917	7.53	4975	51
HR4608	+0.53	1.6	4887	7.07	-0.04	4818	7.01	+0.04	4853	7.04	4853	35
HR5340	-0.20	0.8	4285	6.95	+0.04	4244	6.93	+0.06	4321	6.96	4283	39

<sup>a</sup>Adopted distance modulus of 15.89 mag,  $d = 15.1$  kpc.

<sup>b</sup>Adopted distance modulus of 12.78 mag,  $d = 3.6$  kpc.

Table 9. Final Parameters and Abundances

Name	$T_{\text{eff}}$	$\sigma T$	$\log g$	$[\text{m}/\text{H}]^{\text{a}}$	$v_{\text{t}}$	$\sigma v_{\text{t}}$	$\epsilon(\text{FeI})$	$\sigma\epsilon(\text{FeI})$	$\text{N}(\text{FeI})$	$\epsilon(\text{FeII})$	$\sigma\epsilon(\text{FeII})$	$\text{N}(\text{FeII})$	$\Delta(\text{II-I})$	$\sigma\Delta(\text{II-I})$
BAADE's WINDOW BULGE STARS														
I-012	4257	46	1.55	-0.37	1.54	0.03	7.08	0.08	112	7.14	0.07	4	+0.06	0.11
I-025	4340	21	2.02	+0.51	1.62	0.05	7.96	0.09	90	8.00	0.07	5	+0.04	0.11
I-039	4386	39	2.13	+0.50	1.47	0.06	7.95	0.09	83	7.92	0.07	3	-0.03	0.11
I-141	4335	42	1.68	-0.27	1.33	0.05	7.18	0.09	99	7.20	0.03	4	+0.02	0.10
I-151	4405	28	1.70	-0.78	1.22	0.06	6.67	0.08	83	6.67	0.06	3	-0.00	0.10
I-152	4646	32	2.20	-0.01	1.22	0.06	7.44	0.10	78	7.44	0.06	3	-0.00	0.11
I-156	4312	17	1.74	-0.71	1.16	0.05	6.74	0.07	79	6.76	0.03	4	+0.02	0.08
I-158	4349	18	1.93	-0.20	1.27	0.06	7.25	0.10	102	7.20	0.06	4	-0.05	0.11
I-194	4176	36	1.65	-0.25	1.34	0.05	7.20	0.10	96	7.17	0.09	3	-0.03	0.13
I-202	4184	21	1.53	+0.16	1.12	0.04	7.61	0.11	107	7.58	0.09	4	-0.03	0.14
I-264	4097	14	0.87	-1.15	1.67	0.10	6.30	0.08	83	6.32	0.08	5	+0.02	0.12
I-322	4106	69	0.89	-0.25	1.63	0.04	7.20	0.09	103	7.16	0.05	5	-0.05	0.11
II-033	4277	29	1.41	-0.75	1.41	0.03	6.70	0.07	92	6.71	0.03	4	+0.01	0.07
II-119	4554	57	1.66	-1.22	1.24	0.13	6.23	0.10	58	6.20	0.06	4	-0.03	0.11
II-154	4650	17	2.03	-0.61	1.00	0.05	6.84	0.08	83	6.84	0.07	5	-0.00	0.10
II-172	4480	47	2.14	-0.30	1.03	0.05	7.15	0.11	97	7.22	0.06	5	+0.06	0.13
III-152	4157	8	1.58	-0.41	1.21	0.04	7.04	0.08	103	7.04	0.06	4	+0.00	0.10
III-220	4550	13	1.99	-0.31	1.27	0.01	7.14	0.08	94	7.14	0.08	3	+0.00	0.11
IV-003	4433	5	1.41	-1.29	1.35	0.11	6.16	0.07	58	6.16	0.07	4	-0.00	0.10
IV-047	4556	36	2.28	-0.40	1.54	0.06	7.05	0.11	85	7.10	0.04	4	+0.05	0.11
IV-072	4272	26	1.78	+0.26	1.31	0.05	7.71	0.10	91	7.72	0.02	3	+0.02	0.10
IV-167	4301	22	2.07	+0.46	1.38	0.05	7.91	0.10	89	7.94	0.05	4	+0.03	0.12
IV-203	3902	59	0.51	-1.29	1.88	0.09	6.16	0.07	80	6.32	0.03	4	+0.16	0.07
IV-325	4289	23	2.05	+0.28	1.69	0.05	7.73	0.09	95	7.77	0.05	5	+0.04	0.10
IV-329	4197	23	1.29	-0.94	1.47	0.04	6.51	0.06	77	6.55	0.04	5	+0.04	0.07
BAADE's WINDOW NON-BULGE STARS														
II-122	3912	59	0.14	-0.79	1.53	0.05	6.66	0.09	69	6.70	0.07	4	+0.04	0.12

Table 9—Continued

Name	$T_{\text{eff}}$	$\sigma T$	$\log g$	$[\text{m}/\text{H}]^{\text{a}}$	$v_{\text{t}}$	$\sigma v_{\text{t}}$	$\epsilon(\text{FeI})$	$\sigma\epsilon(\text{FeI})$	$N(\text{FeI})$	$\epsilon(\text{FeII})$	$\sigma\epsilon(\text{FeII})$	$N(\text{FeII})$	$\Delta(\text{II-I})$	$\sigma\Delta(\text{II-I})$
IV-025	4614	66	2.64	+0.21	1.12	0.07	7.66	0.11	99	7.64	0.05	4	-0.03	0.12
LOCAL DISK STARS														
HR1184	4753	11	2.27	-0.38	1.39	0.10	7.07	0.09	122	7.06	0.08	5	-0.01	0.12
HR1346	4823	50	2.43	+0.15	1.57	0.04	7.60	0.09	113	7.59	0.03	5	-0.01	0.09
HR1348	4409	44	1.96	-0.36	1.56	0.04	7.09	0.09	126	7.10	0.04	5	+0.01	0.10
HR1409	4838	49	2.52	+0.20	1.63	0.04	7.65	0.09	118	7.70	0.06	5	+0.05	0.11
HR1411	4961	63	2.69	+0.17	1.48	0.05	7.62	0.08	109	7.65	0.04	4	+0.03	0.09
HR1585	4333	39	1.63	-0.35	1.66	0.04	7.10	0.08	98	7.06	0.02	5	-0.04	0.09
HR2035	4624	34	2.32	-0.64	1.15	0.05	6.81	0.07	122	6.82	0.07	5	+0.01	0.10
HR2113	4277	46	1.37	-0.64	1.57	0.03	6.81	0.07	125	6.73	0.04	5	-0.08	0.08
HR2443	4429	33	1.50	-0.21	1.61	0.03	7.24	0.07	124	7.20	0.04	5	-0.04	0.08
HR3418	4470	70	1.91	+0.16	1.77	0.04	7.61	0.08	105	7.68	0.05	5	+0.07	0.10
HR3733	5001	50	2.89	-0.12	1.50	0.00	7.33	0.08	121	7.40	0.07	5	+0.07	0.11
HR3905	4531	13	2.34	+0.32	1.50	0.00	7.77	0.09	106	7.78	0.06	5	+0.02	0.11
HR4104	4046	10	1.07	-0.36	1.87	0.05	7.09	0.10	101	7.13	0.03	5	+0.04	0.10
HR4382	4475	72	1.72	-0.54	1.55	0.05	6.91	0.10	125	6.94	0.05	5	+0.03	0.11
HR4450	4975	51	2.53	+0.13	1.39	0.07	7.58	0.10	111	7.55	0.10	4	-0.03	0.14
HR4608	4853	35	2.46	-0.41	1.44	0.06	7.04	0.09	123	7.05	0.08	5	+0.01	0.12
HR5340	4283	39	1.55	-0.50	1.61	0.03	6.95	0.07	136	6.99	0.05	5	+0.04	0.08

<sup>a</sup>The value of  $[\text{m}/\text{H}]$  assumes a solar  $\log \epsilon(\text{Fe}) = 7.45$ . The Kurucz and Castelli grids used in this paper assume  $\log \epsilon(\text{Fe}) = 7.50$ . We use atmosphere models with  $\log \epsilon(\text{Fe})$  values picked to match the derived Fe I abundance.

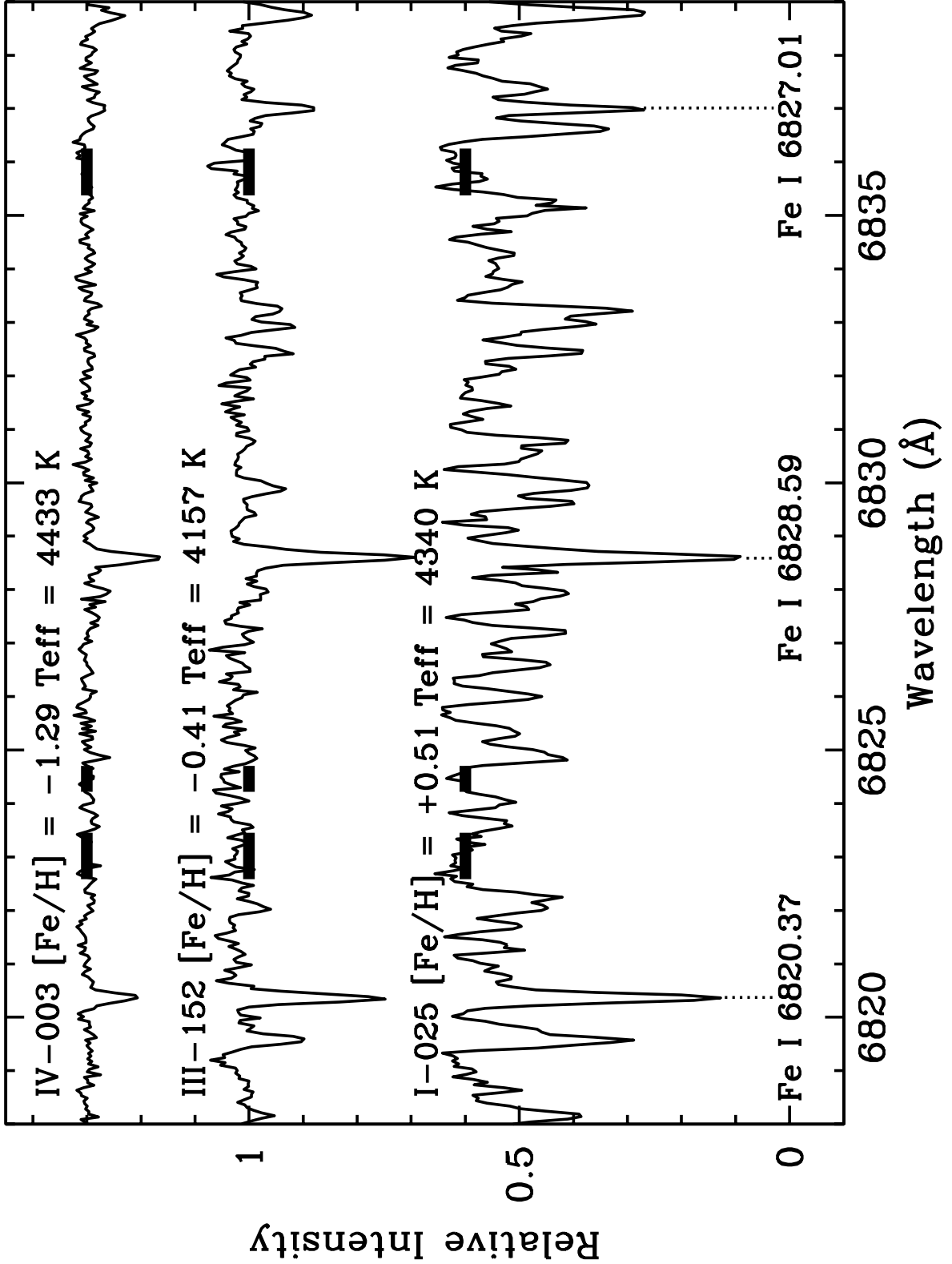


Fig. 1.— Sample spectral region from three stars in the Baade's Window sample. These roughly-normalized Keck/HIRES spectra display the wide range of metallicities seen in the bulge. The signal-to-noise level ranged from about 45 per pixel in I-025 to about 85 per pixel for III-152. Three continuum regions (heavy horizontal bars with arbitrary vertical placement) and three Fe I lines used in the analysis are marked. The spectrum of I-025 demonstrates the sizable line blanketing found in very metal-rich K giants in the bulge. Most of the additional absorption lines in I-025 belong to the CN and Fe lines, and the

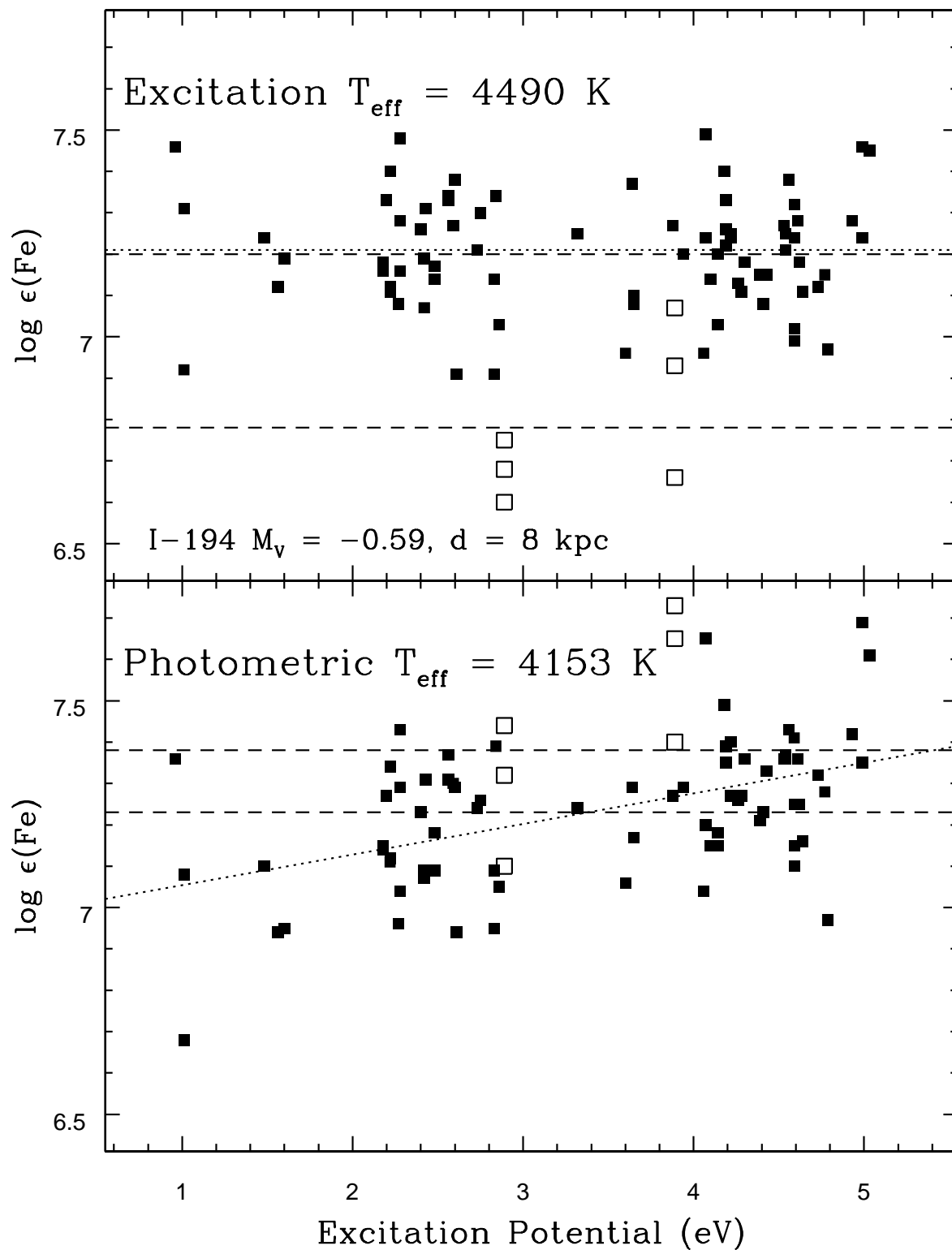


Fig. 2.— Excitation plots for I-194 based on setting the temperature by the slope of the Fe I lines (top panel) or by photometric color (lower panel) and assuming a distance to the star of 8 kpc. Solid points denote Fe I lines, while open points mark the Fe II lines. The two long-dash lines mark the mean values of log  $\epsilon(\text{Fe I})$  and log  $\epsilon(\text{Fe II})$ , and the short-dash lines marks the slope of log  $\epsilon(\text{Fe I})$  as a function of excitation potential. In both panels, it is clear that we cannot obtain both excitation and ionization equilibrium using the line list and analysis method adopted for this example. New line lists and analysis techniques

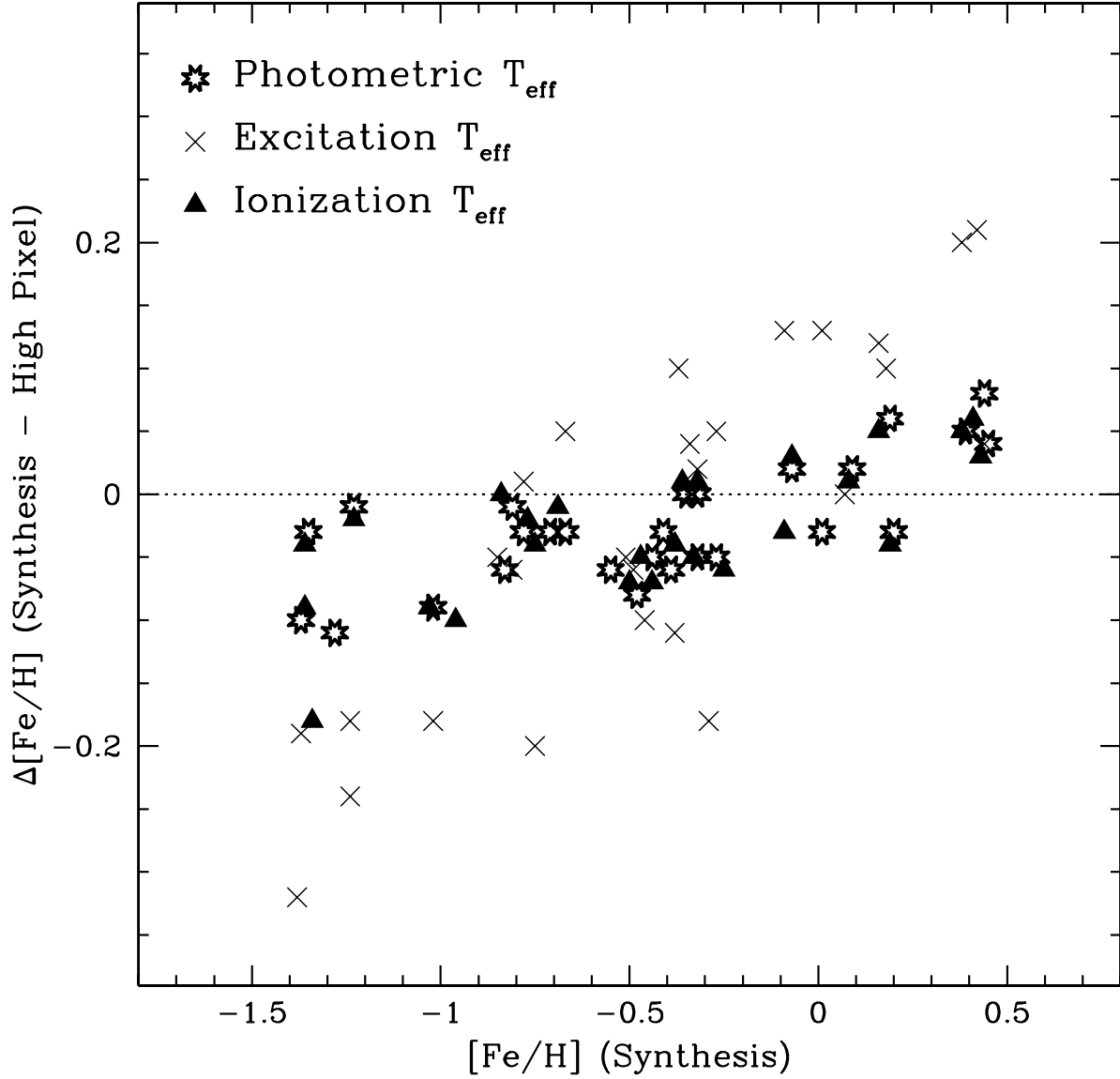


Fig. 3.— The difference in the  $[\text{Fe I}/\text{H}]$  abundances resulting from the two continuum setting methods for each of the 3 stellar temperature methods. The “High Pixel” method exaggerates the potential systematic errors when setting the continuum, but is not unlike the methods used (successfully) on weaker-lined stars. The  $T_{\text{Phot}}$  and  $T_{\text{Ion}}$  methods show only a slight trend with  $[\text{Fe}/\text{H}]$ , but the  $T_{\text{Ex}}$  method shows larger differences as a function of metallicity. The increased slope is primarily due to the correlation between line excitation potential and line strength.

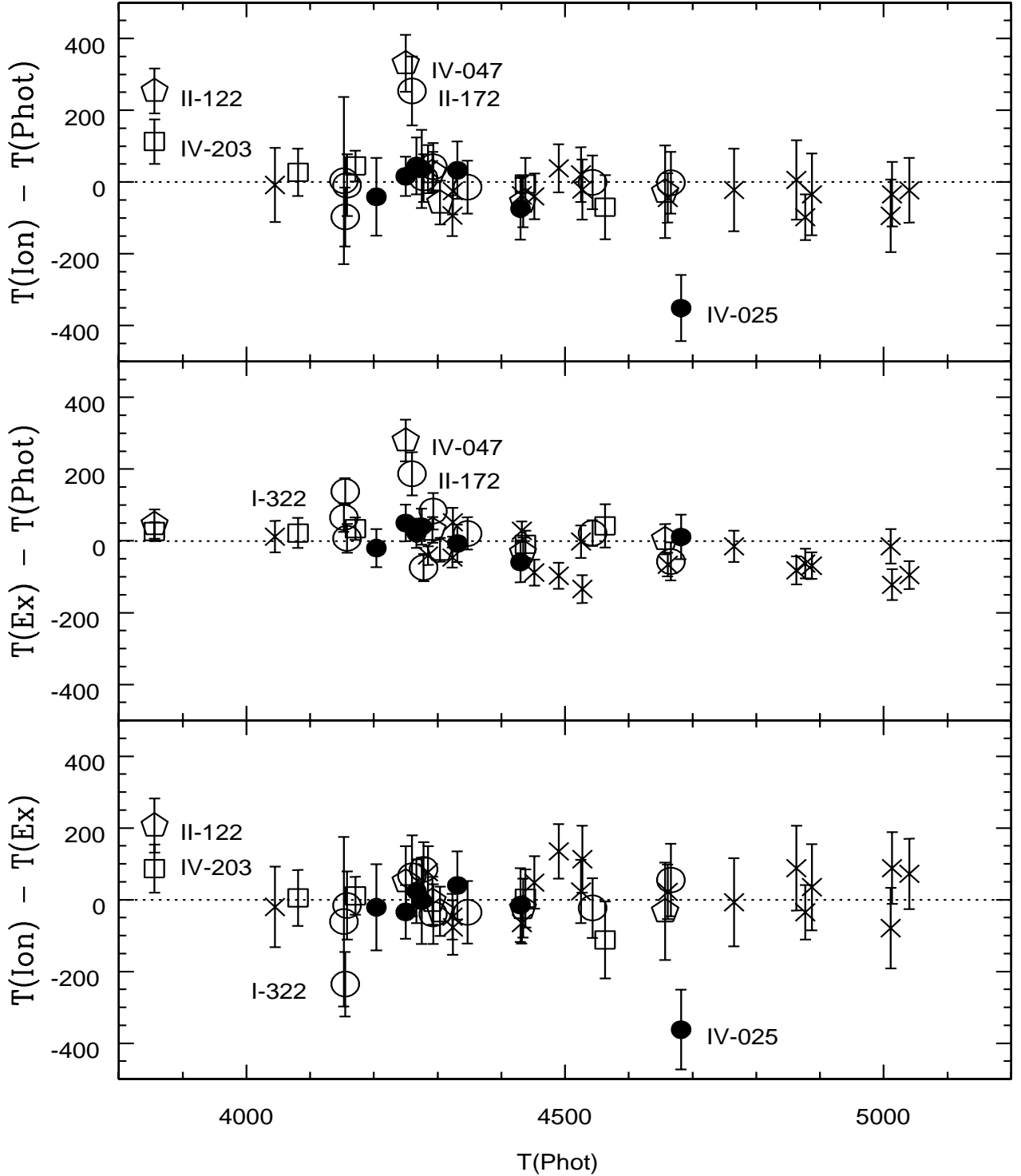


Fig. 4.— Differences between the various stellar temperatures determined by the photometric, excitation, and ionization methods for both the disk and Baade's Window samples. The disk giants are marked by crosses while the Baade's Window giants are marked by symbols representing their metallicity range: solid circles for stars with  $[\text{Fe}/\text{H}] \geq 0.0$ , open circles for stars with  $-0.50 \leq [\text{Fe}/\text{H}] < 0.0$ , open pentagons for stars with  $-1.0 \leq [\text{Fe}/\text{H}] < -0.5$ , and open squares for stars with  $[\text{Fe}/\text{H}] < -1.0$ . The surface gravities used for these determinations were set by assuming a distance of 8 kpc for the Baade's Window sample. The disk stars and most of the Baade's Window sample show excellent agreement between all three methods. The success of the disk giant analysis helps show that our methods work well when well-determined inputs (distance, reddening,

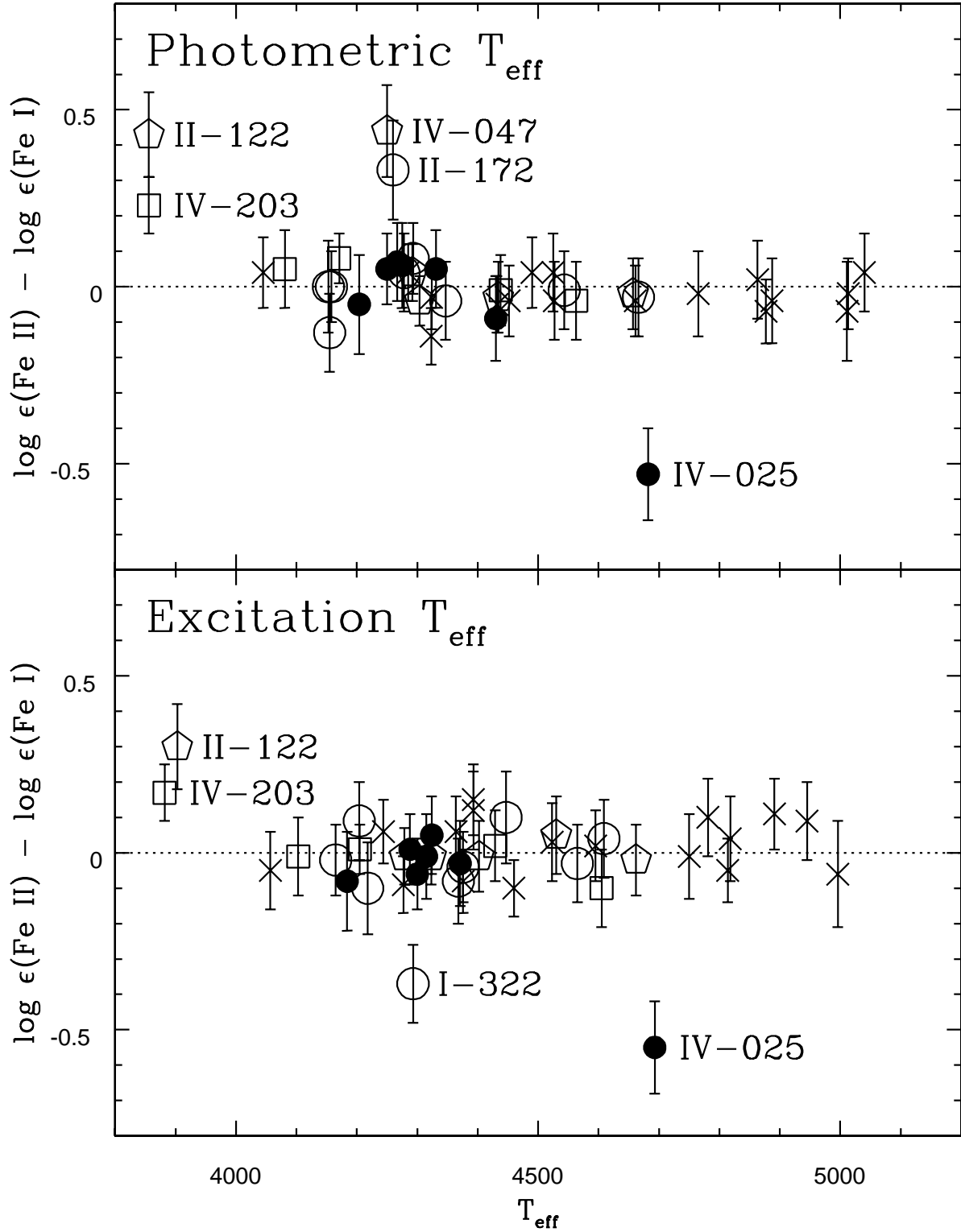


Fig. 5.— Ionization differences plotted as a function of  $T_{\text{eff}}$  for the photometric and excitation temperatures methods. The symbols are the same as those used in Figure 4. The surface gravities used for these determinations were set by assuming a distance of 8 kpc for the Baade’s Window sample. The disk stars and most of the Baade’s Window sample show small ionization differences independent of method. The six exceptions from the Baade’s Window sample that are discussed in the text are marked.

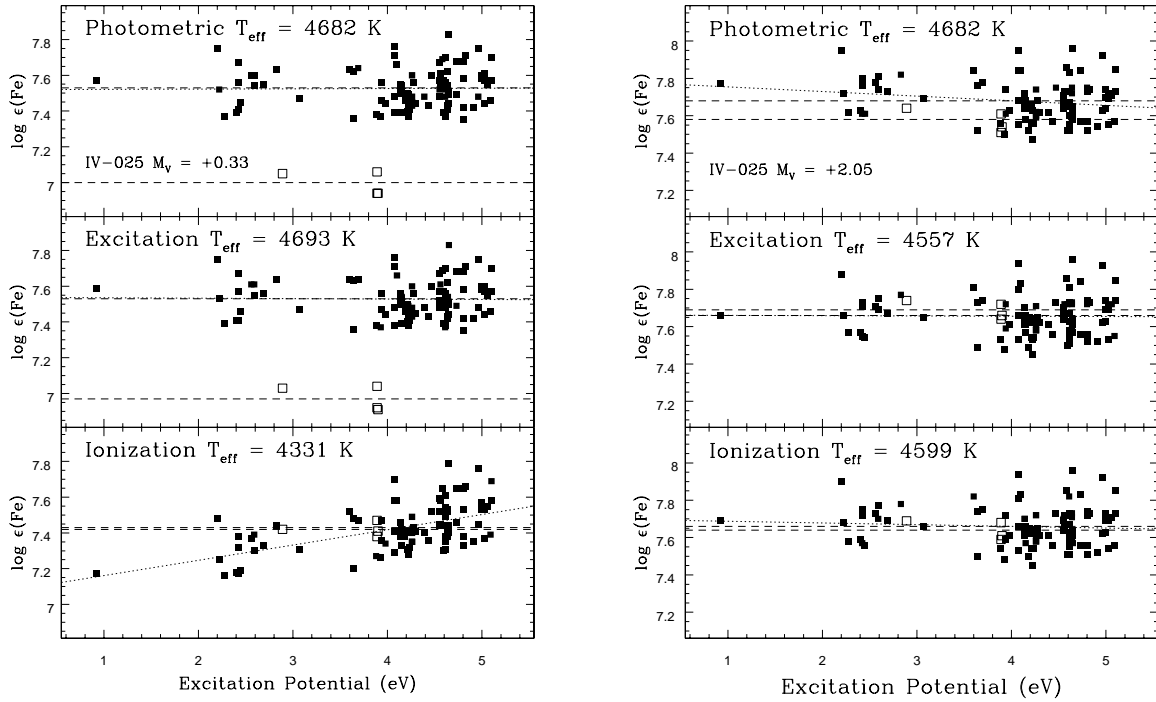


Fig. 6.— Excitation plots for the three different temperature methods for the Baade’s Window star IV-025. The solid points mark individual Fe I lines, while the open points mark Fe II lines. The two long-dash lines mark the mean values of  $\log \epsilon(\text{Fe I})$  and  $\log \epsilon(\text{Fe II})$ , and the short-dash lines marks the slope of  $\log \epsilon(\text{Fe I})$  as a function of excitation potential. The left panel shows the plots for an assumed distance modulus of 14.51 mag (8.0 kpc). The ionization difference for the  $T_{\text{Phot}}$  and  $T_{\text{Ex}}$  methods are  $-0.53$  and  $-0.55$  dex, respectively. The right panel shows the same plots when the distance modulus is changed to 12.79 mag (3.6 kpc). This distance minimizes the ionization and  $T_{\text{eff}}$  differences.

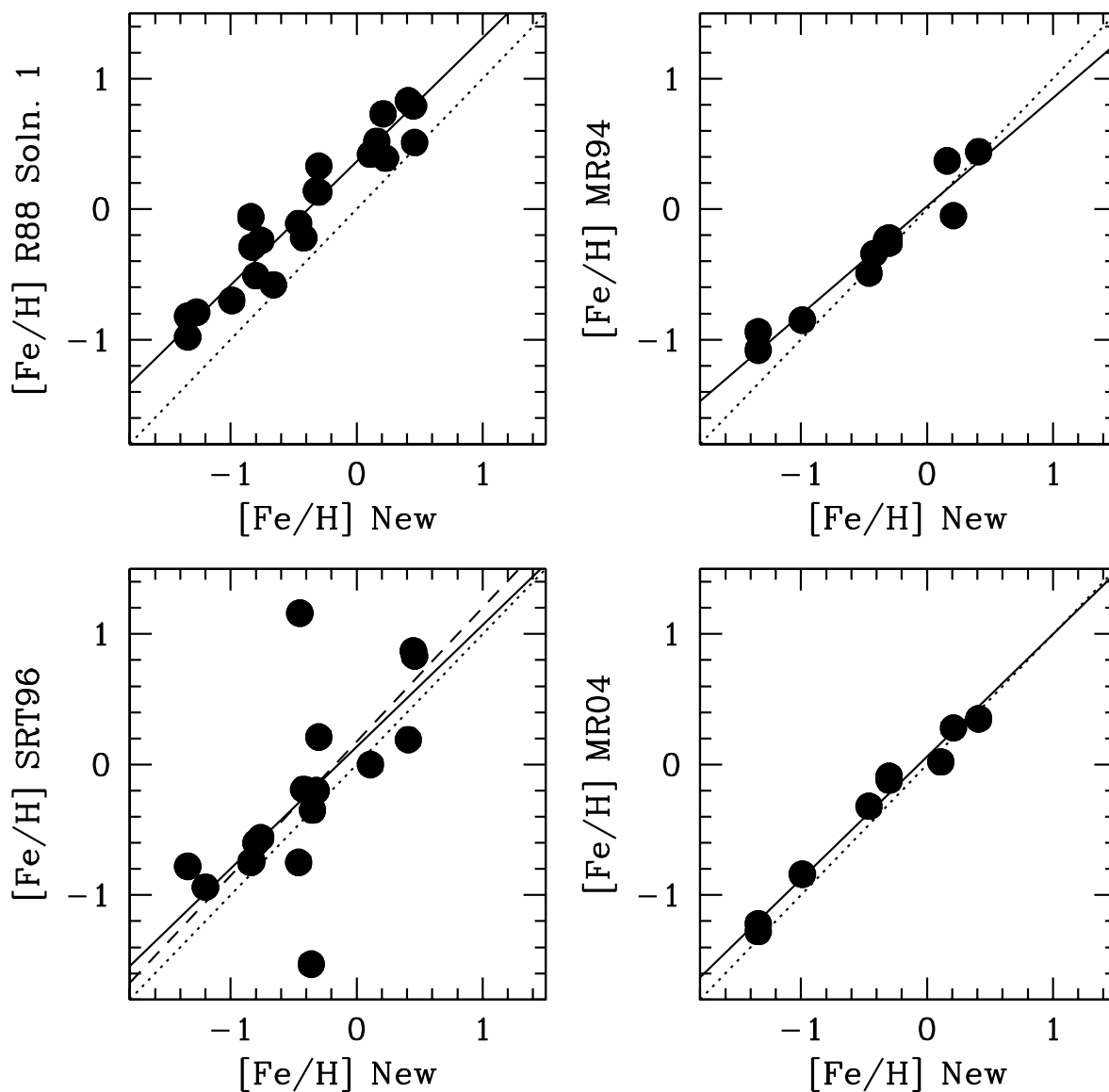


Fig. 7.— Comparison of the  $[\text{Fe}/\text{H}]$  values determined in this work to previous studies of bulge stars (Rich 1998 = R98, McWilliam & Rich 1994 = MW94, Sadler et al. 1996 = SRT96, and McWilliam & Rich 2003 = MR04). The dotted lines are the one-to-one line, and the solid lines are the least-squares fits given in Section 7.3. For the fits to the SRT96 data, the dashed line is the fit to all 17 stars (Equation 6), while the solid line is the fit when the two outlier stars are removed from the sample (Equation 10).

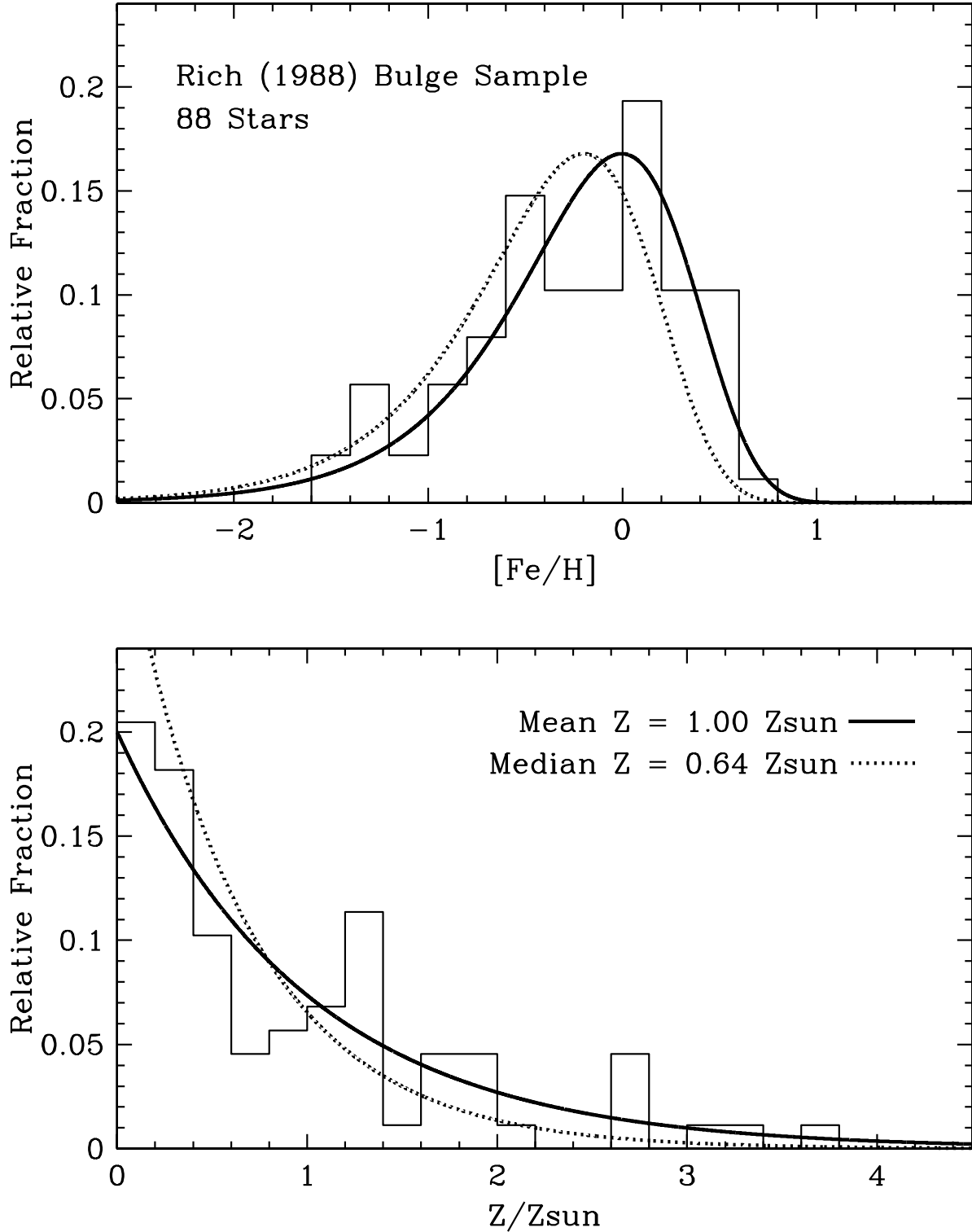


Fig. 8.— Histograms of the  $[\text{Fe}/\text{H}]$  value (top) and heavy metal mass fraction values ( $Z$ ) (bottom) for the recalibrated data of Rich 1988. The recalibration assumes solar abundance ratios for all the heavy elements. Previous high-resolution studies have found that bulge stars have enhanced  $[\text{X}/\text{Fe}]$  ratios for several elements, so the values of  $Z$  are probably lower limits. The two lines are the closed box gas exhaustion model where the value of the yield is either the mean or median  $Z$  value.

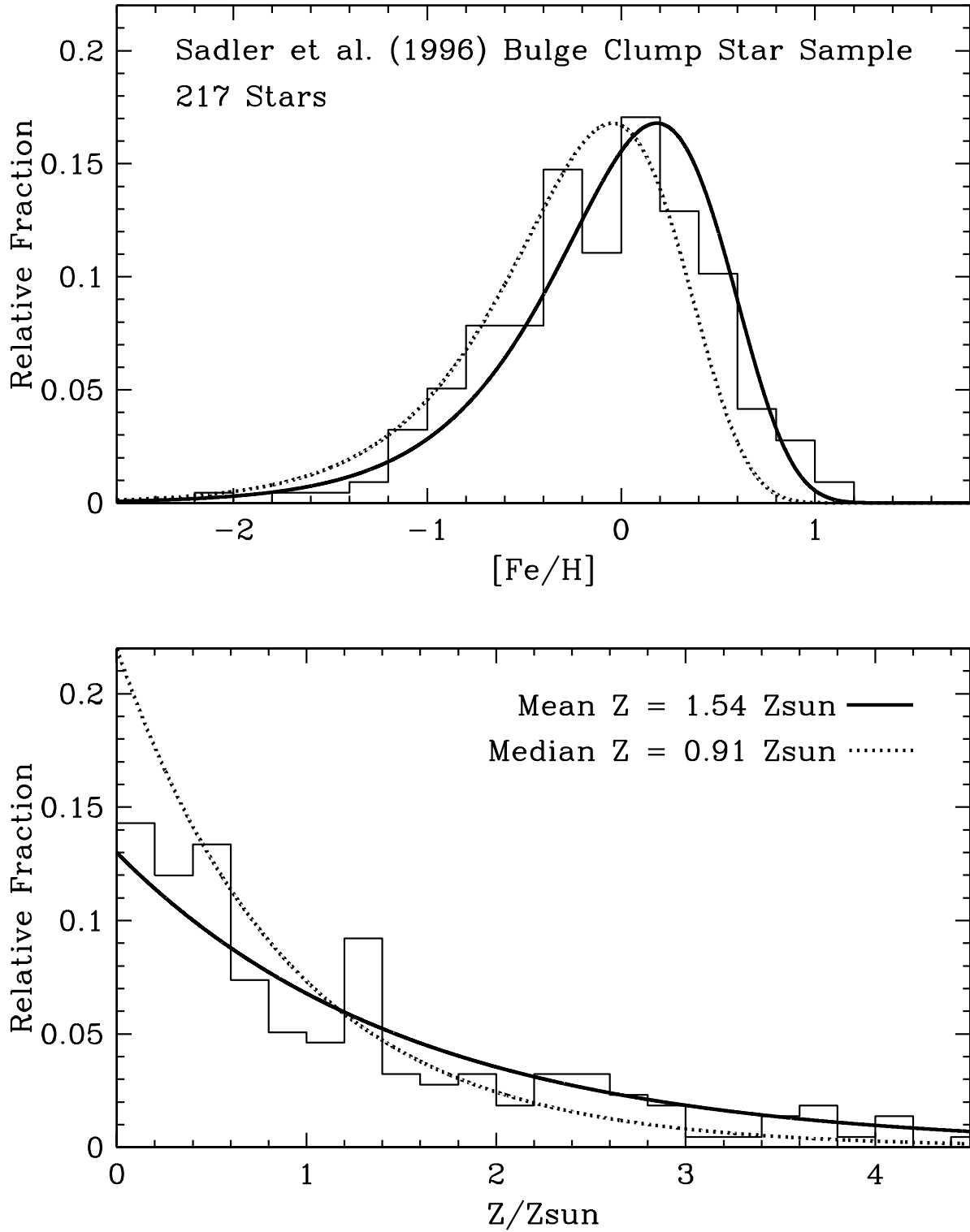


Fig. 9.— Same as Figure 8, except for the recalibrated RGB clump star data of Sadler et al. 1996. The recalibrated data shows more metal-rich stars than the recalibrated R88 sample. There is a wider difference between the mean and median values of  $Z$ , and the best yield for the closed box model most likely falls between the two.

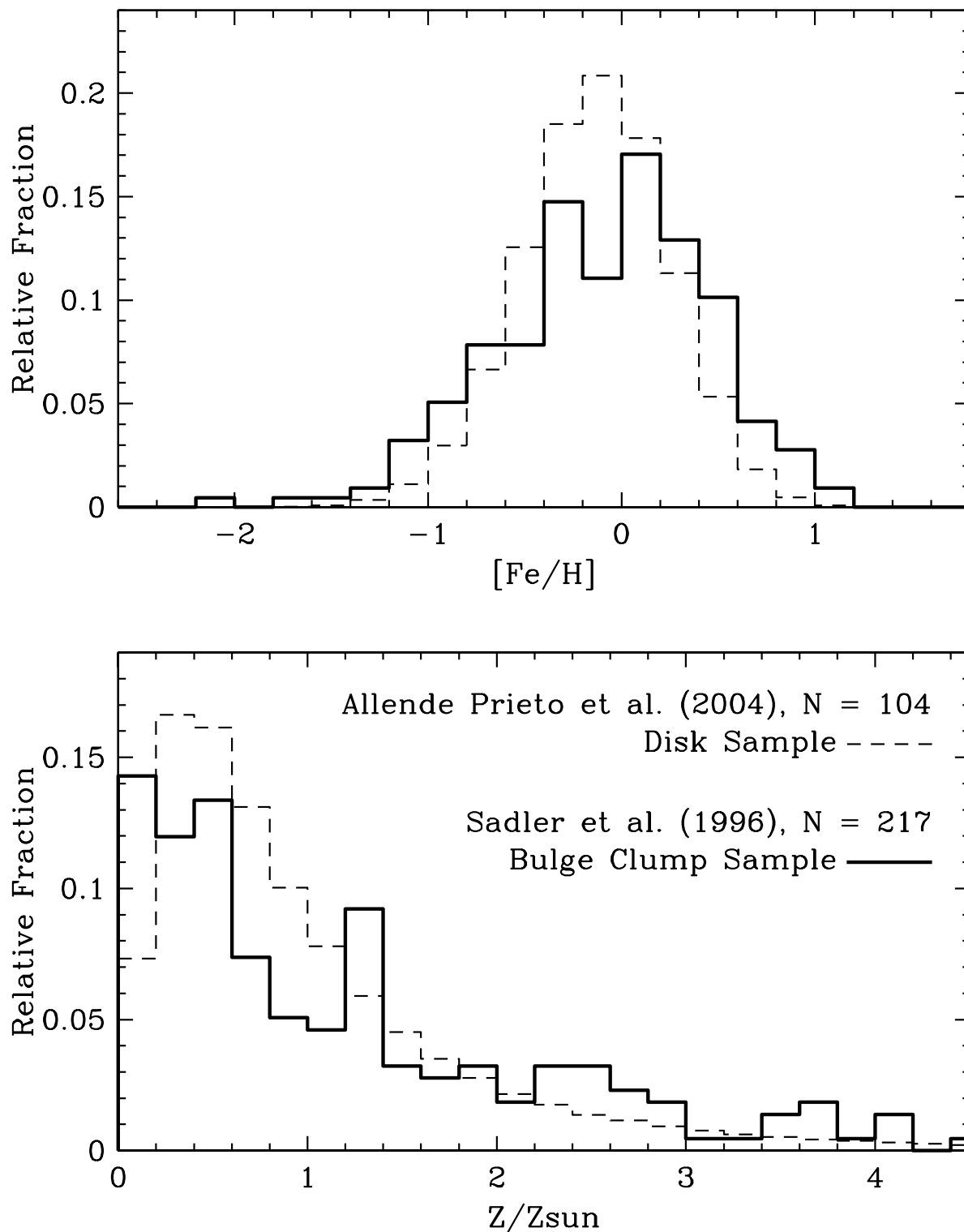


Fig. 10.— Histogram of  $[\text{Fe}/\text{H}]$  values (top) and  $Z$  values (bottom) for the recalibrated RGB clump star data of Sadler et al. 1996 and the solar neighborhood sample of Allende Prieto et al. 2004. The disk sample has been convolved with a Gaussian with  $\sigma = 0.283$  dex in order to degrade the quality of the abundance determinations to the same quality as the SRT96 recalibration. In the top panel, the bulge sample shows a slightly higher mean Fe abundance and a wider spread in metallicity. In the bottom panel, the disk sample shows a drop in the relative fraction in the most metal-poor bin, but an exponential tail